Pharmacological signature and target-specificity of inhibitory circuits formed by Martinotti cells in the mouse barrel cortex

Cristina Donato, Daniella Balduino Victorino, Carolina Cabezas, Andrea Aguirre, Joana Lourenço, Marie-Claude Potier, Javier Zorrilla de San Martin, Alberto Bacci

JNeurosci
THE JOURNAL OF NEUROSCIENCE

Research Articles: Cellular/Molecular

Pharmacological signature and target-specificity of inhibitory circuits formed by Martinotti cells in the mouse barrel cortex

https://doi.org/10.1523/JNEUROSCI.1661-21.2022

Cite as: J. Neurosci 2022; 10.1523/JNEUROSCI.1661-21.2022

Received: 11 August 2021
Revised: 13 September 2022
Accepted: 26 October 2022

Pharmacological signature and target-specificity of inhibitory circuits formed by Martinotti cells in the mouse barrel cortex

Cristina Donato[1,2], Daniella Balduino Victorino[1], Carolina Cabezas[1], Andrea Aguirre[1], Joana Lourenço[1], Marie-Claude Potier[1], Javier Zorrilla de San Martin[1]*, Alberto Bacci[1]*

[1]Sorbonne Université, Institut du Cerveau - Paris Brain Institute - ICM, Inserm, CNRS, APHP, Hôpital de la Pitié Salpêtrière, Paris, France

[2]Present address: Luxembourg Centre for Systems Biomedicine, University of Luxembourg, Belvaux, 12 L-4367, Luxembourg.

Corresponding authors: alberto.bacci@icm-institute.org; javier.zorrilla@icm-institute.org

***Abbreviated title* (50-character maximum):** Martinotti-mediated target-dependent inhibition.

Number of pages: 38

Number of Figures: 8

Number of tables: 0

Number of words: Abstract: 249 Introduction: 1294 Discussion: 2004

Conflict of Interest: The authors declare no competing financial interests.

Acknowledgments: We thank the ICM technical facilities PHENO-ICMICE, iGENSEQ and ICM.Quant. This work was supported by "Investissements d'avenir" ANR-10-IAIHU-06, BBT-MOCONET1 ; BBT-MOCONET2; Agence Nationale de la Recherche (ANR-13-BSV4-0015-01 ; ANR-16-CE16-0007-02 ; ANR-17-CE16-0026-01 ; ANR-18-CE16-0011-01 ; ANR-20-CE16-0011-01; ANR-12-EMMA-0010;), Fondation Recherche Médicale (Equipe FRM DEQ20150331684 and EQU201903007860), NARSAD independent Investigator Grant and Fondation Lejeune (#1790). CD was supported by the École de Neurosciences de Paris et Île de France (ENP) and by the Labex Bio-Psy. PHENO-ICMICE was supported by two "Investissements d'avenir" (ANR-10-IAIHU-06 and ANR-11-INBS-0011-NeurATRIS) and the "Fondation pour la Recherche Médicale". DBV and JZSM are funded by a postdoctoral research fellowship from Jerome Lejeune Foundation.

Abstract

In the neocortex, fast synaptic inhibition orchestrates both spontaneous and sensory-evoked activity. GABAergic interneurons (INs) inhibit pyramidal neurons (PNs) directly, modulating their output activity and thus contributing to balance cortical networks. Moreover, several IN subtypes also inhibit other INs, forming specific disinhibitory circuits, which play crucial roles in several cognitive functions. Here, we studied a subpopulation of somatostatin (SST)-positive INs, the Martinotti cells (MCs) in layer 2/3 of the mouse barrel cortex (both sexes). MCs inhibit the distal portion of PN apical dendrites, thus controlling dendrite electrogenesis and synaptic integration. Yet, it is poorly understood whether MCs inhibit other elements of the cortical circuits, and the connectivity properties with non-PN targets are unknown. We found that MCs have a strong preference for PN dendrites, but they also considerably connect with parvalbumin (PV)-positive, vasoactive intestinal peptide (VIP)-expressing and layer 1 (L1) INs. Remarkably, GABAergic synapses from MCs exhibited clear cell-type-specific short-term plasticity (STP). Moreover, whereas the biophysical properties of MC-PN synapses were consistent with distal dendritic inhibition, MC-IN synapses exhibited characteristics of fast perisomatic inhibition. Finally, MC-PN connections used α5-containing $GABA_A$ receptors ($GABA_A$Rs), but this subunit was not expressed by the other INs targeted by MCs. We reveal a specialized connectivity blueprint of MCs within different elements of superficial cortical layers. In addition, our results identify α5-$GABA_A$Rs as the molecular fingerprint of MC-PN dendritic inhibition. This is of critical importance, given the role of α5-$GABA_A$Rs in cognitive performance and their involvement in several brain diseases.

Significance statement

Martinotti cells (MCs) are a prominent, broad subclass of SST-expressing GABAergic INs, specialized in controlling distal dendrites of PNs and taking part in several cognitive functions. Here we characterize the connectivity pattern of MCs with other INs in the superficial layers (L1 and L2/3)

of the mouse barrel cortex. We found that the connectivity pattern of MCs with PNs as well as PV, VIP and L1 INs exhibit target-specific plasticity and biophysical properties. The specificity of α5-$GABA_A$Rs at MC-PN synapses, and the lack or functional expression of this subunit by other cell types, define the molecular identity of MC-PN connections and the exclusive involvement of this inhibitory circuits in α5-dependent cognitive tasks.

Introduction

In the neocortex, fast synaptic inhibition underlie important cognitive-relevant activity (Buzsáki, 2010; Isaacson and Scanziani, 2011). Neocortical inhibition is provided by GABAergic INs, which are highly heterogeneous and connect with both principal pyramidal neurons (PNs) and other inhibitory cells in a highly stereotyped manner. Some INs, such as parvalbumin (PV)-expressing basket cells, innervate the perisomatic region of cortical PNs, and they thus provide a tight temporal control of PN spiking output and drive cognition-relevant fast network oscillations, especially in the β-γ-frequency range (20-100 Hz)(Bartos et al., 2007; Buzsáki and Wang, 2012).

Conversely, other interneuron types, such as those expressing the neuropeptide somatostatin (SST), were shown to target dendrites of PNs, thereby controlling dendritic electrogenesis, non-linear integration and glutamatergic synaptic input (Wang et al., 2004; Lovett-Barron et al., 2012; Wilson et al., 2012; Schulz et al., 2018). In sensory cortices, SST INs were shown to be involved in lateral inhibition, playing a major role in key sensory computations, such as surround suppression (Kapfer et al., 2007; Silberberg and Markram, 2007; Berger et al., 2009; Adesnik and Scanziani, 2010; Adesnik et al., 2012). Moreover, SST-operated dendritic inhibition was shown to encode fear memory and affective behavior in prefrontal cortex (Xu et al., 2013; Scheggia et al., 2019; Clem and Cummings, 2020).

SST INs were proposed to be the source of a profuse 'blanket' of inhibition due to their dense connectivity with PNs (Fino and Yuste, 2011). However, this view neglects the diversity of SST-positive INs (Riedemann et al, 2016; Gouwens et al., 2020; Zhou et al., 2020; Bougeon et al., 2022), and the fact that they preferentially contact specific PN subclasses (Hilscher et al., 2016) as well as other inhibitory neurons (Pfeffer et al., 2013; Tremblay et al., 2016). In general, SST INs can be classified as Martinotti cells (MCs) and non-Martinotti cells, which exhibit differential connectivity patterns as well as specific molecular profiles (Wang et al., 2004; Ma et al., 2006; Tremblay et al., 2016; Yavorska and Wehr, 2016; Paul et al., 2017; Scala et al., 2019; Gouwens et al., 2020; Bugeon et

al., 2022). According to the classical description of MCs, these INs exhibit a well-defined axonal morphology, as they project their axons to layer 1, where they extensively inhibit the most distal dendritic tufts of PNs (Wang et al., 2004; Ma et al., 2006; Kapfer et al., 2007; Silberberg and Markram, 2007; Tremblay et al., 2016). Functionally, MCs are efficiently recruited by local PNs with loose-coupled, strongly facilitating synapses (Reyes et al., 1998; Wang et al., 2004; Kapfer et al., 2007; Silberberg and Markram, 2007), and are inhibited by vasoactive intestinal peptide (VIP)-expressing GABAergic INs (Pfeffer et al., 2013; Karnani et al., 2016; Tremblay et al., 2016; Walker et al., 2016). Finally, MCs form synapses with other elements of the cortical circuit, namely other inhibitory INs (Ma et al., 2006; Pfeffer et al., 2013). However, the actual extent and biophysical properties of these disinhibitory circuits are unknown and/or generalized over SST-expressing MCs and non-MCs (Pfeffer et al., 2013).

Importantly, dendritic inhibition provided by MC-PN synapses is mediated by α5-containing $GABA_AR$ (α5-$GABA_ARs$) (Ali and Thomson, 2008; Zorrilla De San Martin et al., 2020). Similarly, in the hippocampus, dendritic inhibitory synapses from SST-positive INs onto PNs express functional α5-$GABA_ARs$ (Schulz et al., 2018). This prompts the question whether GABAergic synapses formed by MCs onto other elements of the cortical circuit use this specific subunit of $GABA_ARs$. Understanding the actual synaptic circuits relying on the α5 subunit has important clinical implications. Indeed, α5-$GABA_ARs$ were indicated as a prominent target for therapeutic interventions for cognitive dysfunctions in Down syndrome (Braudeau et al., 2011; Duchon et al., 2019; Schulz et al., 2019; Zorrilla De San Martin et al., 2020), depression (Zanos et al., 2017), anesthesia-induced memory impairment (Zurek et al., 2014) and schizophrenia (Duncan et al., 2010; Gill and Grace, 2014). Recent studies described the large diversity of SST-expressing INs (Riedemann et al., 2016; Paul et al., 2017; Gouwens et al., 2020; Zhou et al., 2020; Bugeon et al., 2022) and proposed a number of genetically, morphologically and functionally defined sub-classes highlighting the need for genetic tools to assess the function of these sub-groups. Indeed, presently, there are no specific mouse lines that allow the

identification and/or manipulation of specific subtypes of SST-expressing INs, including the several subclasses of MCs.

Here we used a transgenic mouse line (*Gad1-GFP,* line X98 (Ma et al., 2006)) to assess the connectivity of GFP-expressing MCs (herein defined X98 MCs) in the superficial layers of the mouse barrel cortex. Using this tool, we found that, in addition to the known connectivity with PN distal dendrites, X98 MCs connect extensively also with PV, VIP and L1 INs, but not with other X98 MCs. Interestingly, GABAergic synapses formed by X98 MCs exhibited clear target specificity of STP. Finally, dendritic inhibition using α5-$GABA_A$Rs is a peculiarity of X98 MC-PN synapses, as unitary responses from X98 MCs to other INs exhibited fast (<1ms) rise-time, and they were not modulated by a α5 negative allosteric modulator (NAM).

Altogether, these results indicate the pharmacological, connectivity and biophysical fingerprint used by X98 MCs for inhibitory synapses that they make with PNs and other elements of the cortical circuit.

Materials and Methods

Animals

Experimental procedures followed national and European (2010/63/EU) guidelines and have been approved by the author's institutional review boards and national authorities. All efforts were made to minimize suffering and reduce the number of animals. Mice used in this study were of both sexes. In order to identify GABAergic transmission from different INs we used several mouse models. To record from PV INs, we initially crossed *Pvalb*-cre mice (Jackson Laboratory, Strain Number: 008069) with a mouse line that expresses a *loxP*-flanked STOP cassette preventing the transcription of a CAG promoter-driven red fluorescent protein variant (tdTomato) (Jackson Laboratory, Strain Number: 007909). Following Cre-mediated recombination, the resulting mice exhibit robust

tdTomato fluorescence in PV INs. In the experiments illustrated in Figs. 2 and 5, we used PValbTomato mouse line (Kaiser et al., 2016, Jackson Stock# 27395), a line that expresses TdTomato fluorescent protein specifically in PV INs. To record from MCs, we used GAD-67-GFP mice, line X98 (Ma et al., 2006, herein defined as X98; Jackson Laboratory Stock# 006340). To perform simultaneous recordings from X98 MCs and PV INs we crossed X98 mice with PValb-tdtomato. Furthermore, in order to record from synaptically connected VIP INs and X98 MCs, we crossed VIP-Cre mice (Jackson Laboratory, Strain Number: 010908) with X98 mice (herein defined as VIPcre::X98 mice) and infected newborns with viral vectors carrying the genes of either channelrhodopsin-2 (ChR2) or TdTomato (see below details of different viral infections).

In Vitro Slice Preparation and Electrophysiology

Coronal slices (300-350 µm thick) from somatosensory cortex were obtained from 18- to 25-d-old mice. This range of ages was chosen to find a compromise between INs maturation (reached before P25 in the somatosensory cortex; Okaty et al., 2009; Goldberg et al., 2011) and experimental yield. The yield of finding connected pairs of neurons in the cortex decrease starkly with age, notably after postnatal day 25, thus reducing substantially the feasibility of pharmacological treatments during pair recordings in the different mouse lines used in this study. Animals were deeply anesthetized with isoflurane and decapitated. Brains were quickly removed and immersed in "cutting" solution (4°C) containing the following (in mM): 126 choline, 11 glucose, 26 $NaHCO_3$, 2.5 KCl, 1.25 NaH_2PO_4, 7 $MgSO_4$ and 0.5 $CaCl_2$ (equilibrated with 95-5% O_2-CO_2, respectively). Slices were cut with a vibratome (Leica) in the same cutting solution and then incubated in oxygenated artificial cerebrospinal fluid (aCSF) containing the following (in mM): 126 NaCl, 2.5 KCl, 2 $CaCl_2$, 1 $MgSO_4$, 1.25 mM NaH_2PO_4, 26 mM $NaHCO_3$, and 16 mM glucose (pH 7.4), initially at 34°C for 30 min, and subsequently at room temperature until transfer to the recording chamber. Recordings were obtained at 32-34°C. Whole-cell voltage-clamp recordings were performed in from layer (L)2/3 PNs, MCs, PV, VIP INs and L1 INs

of the primary somatosensory cortex. PNs were visually identified using infrared video microscopy by their large somata and pia-oriented apical dendrites. L1 INs were also visually identified with transmitted light only as they are the only cell type with the soma present in L1. MCs (labeled with GFP, see Fig 1), VIP INs and PV INs (labeled with TdTomato), were identified using LED illumination (blue, λ=470nm, green λ=530nm, OptoLED system, Cairn Research, Faversham, UK) coupled to epifluorescent optical pathway of the microscope. Single or double voltage-clamp whole-cell recordings were made with borosilicate glass capillaries (with a tip resistance of 2–4 MΩ) filled with different intracellular solutions depending of the experiment. For unitary inhibitory postsynaptic currents (uIPSCs) the intracellular solution contained (in mM): 70 K-gluconate, 70 KCl, 10 HEPES, 1 EGTA, 2 MgCl2, 4 Mg-ATP, 0.3 Na-GTP, pH adjusted to 7.2 with KOH, 280–300 mOsm or 145 CsCl, 4.6 $MgCl_2$, 10 HEPES, 1 EGTA, 0.1 $CaCl_2$, 4 Na-ATP, 0.4 Na-GTP, pH adjusted to 7.2 with CsOH, 280–300 mOsm. To confirm the GABAergic nature of uIPSCs, gabazine (10 μM) was added to the aCSF at the end in some experiments. For tonic inhibition experiments, GABA (5 μM) was added to the aCSF. To record unitary excitatory postsynaptic currents (uEPSCs) from INs, a low chloride intracellular solution was used and DNQX was omitted in the aCSF superfusate. In these experiments, the intracellular solution had the following composition (in mM): 150 K-gluconate, 4.6 $MgCl_2$, 10 HEPES, 1 EGTA, 0.1 $CaCl_2$, 4 Na-ATP, 0.4 Na-GTP, pH adjusted to 7.2 with KOH, 280–300 mOsm. In voltage-clamp experiments, access resistance was on average <15 MΩ and monitored throughout the experiment. Recordings were discarded from analysis if the resistance changed by >20% over the course of the experiment. Unclamped action currents in presynaptic neurons were elicited in voltage-clamp mode by brief (1 ms) somatic depolarizing steps (from -70 to 0 mV). This resulted in unitary synaptic transmission in simultaneously recorded postsynaptic neurons. A train of 5 presynaptic action currents at 50 Hz was applied to infer STP of synaptic responses. The paired pulse ratio (PPR) was obtained as the peak amplitude of the second uEPSC divided by that of the first. In order to isolate $GABA_A$-receptor-mediated currents, DNQX (10 μM) was present in the superfusate of all experiments, unless otherwise indicated.

Signals were amplified, using a Multiclamp 700B patch-clamp amplifier (Molecular Devices, San Jose, CA), sampled at 20-100 kHz and low-pass filtered at 4 KHz (for voltage clamp experiments) and 10 KHz (for current clamp experiments). All drugs were obtained from Tocris Cookson (Bristol, UK) or Sigma (St. Louis, MO, USA). α5IA, (3-(5-methylisoxazol-3-yl)-6-[(1-methyl-1,2,3-triazol-4-yl)methyloxy]-1, 2, 4-triazolo[3, 4-a]phthalazine) also named L-822179 was synthesized by Orga-Link SARL (Magny-les-Hameaux, France) according to Sternfeld et al. (2004) as in Braudeau et al. (2011). The hydrochloride salt was solubilized in DMSO at a concentration of 1mM and then diluted in the appropriate buffer.

Virus-Mediated Gene Delivery and Optogenetics

To study X98 MC-VIP and VIP- X98 MC synapses we first crossed crossed VIPcre with X98 mice and injected 300 nL of a solution containing adeno-associated viral (AAV) particles into the somatosensory cortex of ice–anesthetized pups (P0–3) to selectively express TdTomato or channelrhodopsin-2 (ChR2) in VIP INs. Injections were made with a beveled glass pipette 300 µm deep in the somatosensory cortex through intact skin and skull. We then delivered the solution containing the AAVs using a Nanoliter 2000 Injector (WPI Inc., Sarasota, FL, USA)). The pipette was left in place for an additional 30 s, before being retracted. The AAVs expressed floxed ChR2 or TdTomato (AAV9.EF1.dflox.hChR2(H134R)-mCherry.WPRE.hGH; Addgene #20297 and pAAV-FLEX-tdTomato; Addgene #28306, respectively) purchased from the Penn Vector Core (University of Pennsylvania). At the end of the procedure, pups were returned to their mother. ChR2 activation was obtained by brief (0.5-2 ms) LED light pulses on cortical slices (λ = 470 nm). Experiments were performed using a 60X water immersion lens. Light-evoked responses were recorded in L 2/3 MCs and were completely abolished by gabazine (not shown).

Data analysis

Experiments on firing dynamics, tonic currents and unitary paired recordings were analyzed with Clampfit (Molecular Devices), Origin (OriginLab Corp., Northampton, MA) and custom-made scripts in Matlab (MathWorks, Inc., Natick, MA, USA). Spontaneous synaptic events were detected using custom written software (Wdetecta, courtesy J. R. Huguenard, Stanford University https://hlab.stanford.edu/wdetecta.php) based on an algorithm that calculates the derivative of the current trace to find events that cross a certain defined threshold (Ulrich and Huguenard, 1996). Amplitude and rise times of the events were then binned and sorted, using other custom written routines (courtesy J. R. Huguenard, Stanford University).

The peak-to-baseline decay phase of uIPSCs was fitted by the following double exponential function:

$$F(\mathrm{t}) = A_{fast}\, e^{\frac{-t}{\tau_{fast}}} + A_{slow}\, e^{\frac{-t}{\tau_{slow}}} \qquad \textit{Equation (1)}$$

where A_{fast} and A_{slow} are the fast and slow amplitude components, and τ_{fast} and τ_{slow} are the fast and slow decay time constants, respectively. The weighted decay time constant ($\tau_{d,w}$) was calculated using the following equation:

$$\tau_{\mathrm{d,w}} = \frac{[(A_{fast} \cdot \tau_{fast}) + (A_{slow} \cdot \tau_{slow})]}{A_{fast} + A_{slow}} \qquad \textit{Equation (2)}$$

The adaptation index was calculated as the last/first inter-spike interval ratio following a train of spikes induced by injection of a depolarizing step of current. Passive properties as well as synaptic currents were analyzed with Clampfit and custom-made scripts in MATLAB (Mathworks). Both unitary and light-induced IPSCs were averaged across at least 20 sweeps for each condition examined. Results are presented as means ± SEM unless otherwise stated.

Morphological reconstruction

To reconstruct and quantify anatomical features of different cortical neurons, biocytin (Sigma; cat num.: B4261) was included in the intracellular solution at a high concentration (10mg/mL), which required extensive sonication. To avoid excessive degradation of fragile molecules such as ATP, sonication was performed in an ice bath. The intracellular solution was then filtered twice to prevent the presence of undissolved lumps of biocytin in the patch pipette. Recordings lasted for at least 30 min. We used a high concentration of biocytin to allow efficient filling of axons from recorded INs, as demonstrated previously (Jiang et al., 2015; Scala et al., 2019). This biocytin concentration did not alter the health of the recorded neuron, the incidence of obtaining high-resistance (>1 GΩ) seals nor the stability of whole-cell recordings. During that time, access resistance was continuously monitored throughout the experiment. At the end of recordings, the patch pipette was removed carefully to obtain an outside-out patch in order to reseal the cell properly. The slice was then left in the recording chamber for a further 5-10 min to allow biocytin diffusion. Slices were then fixed with 4% paraformaldehyde in phosphate buffer saline (PBS, Sigma) for at least 48h. Following fixation, slices were incubated with the avidin-biotin complex (Vector Labs) and a high concentration of detergent (Triton-X100, 5%) for at least two days before staining with 3,3'-Diaminobenzidine (DAB, AbCam). Cells were then reconstructed, and cortical layers delimited using Neurolucida (MBF Bioscience). Neuronal reconstructions were aligned to a mouse atlas from the Allen Institute. By using Neurolucida Explorer, we analyzed the length of axons and dendrites of MCs in L2/3 and L1 of somatosensory cortex. Data were exported and analyzed in OriginPro 2016 (OriginLab Corporation).

Immunofluorescence, confocal imaging, and quantitative imaging analysis

18- to 25-days-old X98 and VIPcre:X98 mice were anesthetized with ketamine/xylazine (8 µl/g mouse of a 100 mg/ml ketamine and 13 mg/ml xylazine mixture) and transcardially perfused with 1X PBS solution containing heparin (5 IU/ml) followed by 4% (PFA) fixative solution in 1X PBS. Next, brains were dissected and post-fixed overnight at 4°C with the same fixative solution. The following

day, brains were placed overnight in a 30% sucrose solution in 1X PBS for cryoprotection and then frozen in isopentane at a temperature <-50°C. Brains were cut into 50-µm-thick coronal sections using a freezing microtome (HM450, ThermoFisher, Waltham, MA, USA) and kept in a 0.4% sodium azide solution at 4°C until immunostaining. For immunostaining for GFP, SST, and PV (Fig. 1*A*), free-floating brain sections were permeabilized with a 0.3% triton X-100 and 10% normal goat serum blocking solution in 1X PBS for 2 hr at room temperature. Brain sections were then incubated overnight at 4°C in a 0.003% triton X-100 and 10% normal goat serum solution containing the primary antibodies anti-GFP guinea pig (1:1000; Synaptic Systems, 132 005), anti-SST mouse (1:1000; Biotechnology, sc-55565), and anti-PV rabbit (1:1000; SWant, PV-28). Brains sections were then washed three times for 10 min in 1X PBS and incubated for 3 hr at room temperature in a 0.003% triton X-100 and 10% normal goat serum solution containing the secondary antibodies goat anti-guinea pig (1:500; Life technologies, A-11073), goat anti-mouse (1:500; Life technologies, A-21052), and goat anti-rabbit (1:500; Life technologies, A-31556), conjugated to Alexa Fluor 488, 633, and 405, respectively. Brains sections were then washed three times for 10 min in 1X PBS and coverslipped with mounting medium (Fluoromount, Sigma Aldrich, F4680). Before proceeding with immunostaining experiments wherein pre and/or postsynaptic markers (i.e., gephyrin and VGAT) were used (Fig. 3), free-floating brain sections were subjected to an antigen retrieval procedure using a citrate-based buffer. Briefly, brain sections were washed twice for 10 min in 1X PBS, transferred to a 0.01 M sodium citrate solution (pH 6), and then heated to and maintained at 95°C in water bath for 5 min. Brain sections were washed three times for 10 min in 1X PBS and then subjected to the above described permeabilization and immunostaining procedures, using different combinations of antibodies as follow: primary antibodies anti-GFP guinea pig (1:1000; Synaptic Systems, 132 005), anti-PV rabbit (1:1000; SWant, PV-28) or anti-PV mouse (1:1000; Sigma Aldrich, P 3088) or anti-DsRed mouse (1:500; Takara Bio Clontech, 632392) or anti-DsRed rabbit (1:500; Takara Bio Clontech, 632496) or anti-NeuN mouse (1:500; Merck, MAB377), and anti-gephyrin mouse (1:1000; Synaptic System, 147011) or anti-VGAT rabbit (1:500; Synaptic System, 131002); and

secondary antibodies goat anti-guinea pig (1:500; Life technologies, A-11073) conjugated to Alexa Fluor 488, goat anti-mouse (1:500; Life technologies, A-21052) or anti-rabbit (1:500; Life technologies, A-21071) conjugated to Alexa Fluor 633, and goat anti-mouse (1:500; Life technologies, A-31553) or anti-rabbit (1:500; Life technologies, A-31556) conjugated to Alexa Fluor 405. The samples were analyzed and images were acquired under a Leica TCS SP8 laser scanning confocal microscope using 405, 488, and 633 nm laser excitation lines in the sequential mode. For the quantification of GFP-, SST-, and PV-positive cells, multiple digital images were captured using a 20x oil-immersion objective lens by a tile scan of the primary somatosensory cortex, which were then combined into a single composite image. The numbers of cells expressing GFP, SST, or PV, as well as double-positive cells for GFP and SST, were manually counted using Cell Counter plugin in ImageJ 1.52a (US National Institutes of Health). For the quantification of vGAT-positive terminals (in apposition to GFP-positive axons/puncta) onto somas immunolabeled with antibody against either PV, TdTomato, or NeuN, z-stack digital images of 3 to 5 fields of view (FOV) in L1 and L2/3 were captured using a 63x oil-immersion objective lens and a zoom factor of 2.5x. PV-, TdTomato-, or NeuN-labeled somas were randomly selected for visual quantification of juxtaposed $VGAT^+$ and GFP^+ puncta. Images were deconvolved using Huygens Essential software (Scientific Volume Imaging, Hiversum, The Netherlands), and orthogonal projections were obtained by the Fiji version of ImageJ 1.52a (US National Institutes of Health).

Statistical Analysis

All statistical analysis were performed in Origin (OriginLab Corp., Northampton, MA). Normality of the data was systematically assessed (Shapiro-Wilk normality test). Normal distributions were statistically compared using Paired t-Test or Two-sample t-Test. When data distributions were not normal or n was small, non-parametric tests were performed (Mann-Whitney, Wilcoxon Signed Ranks Test). Two-way analysis of variance (ANOVA) tests were followed by Bonferroni's multiple

comparison post hoc. Differences were considered significant if p <0.05 (*p<0.05, **p<0.01, ***p<0.001).

Results

The X98 mouse line is a reliable tool to study L2/3 Martinotti cells

Despite being broadly classified as dendrite-targeting INs, SST-expressing cells exhibit significant electrophysiological, anatomical, connectivity and molecular heterogeneity (Ma et al., 2006; Paul et al., 2017; Naka et al., 2019; Gouwens et al., 2020; Bugeon et al., 2022). In order to specifically study the connectivity of L2/3 MCs we searched for a suitable mouse line. X98 are transgenic mice carrying the gene coding for GFP under control of the *Gad1* promoter. GFP is expressed predominantly in cortical layers (L) 5B and 6, and, to a lesser extent, in L2/3 (Ma et al., 2006). However, although GFP-expressing neurons are present in L2/3, these had not been previously analyzed. Therefore, we first set out to confirm that GFP-expressing neurons in L2/3 belong to the SST-positive interneuron subtype, broadly defined as the MC.

We performed immunofluorescence staining on microtome-cut coronal somatosensory slices of 18-25-days-old X98 mice (Fig. 1*A*) and showed that 100% of GFP-expressing neurons also expressed SST, while 32.1 ± 3.4 % of SST-positive, and 100% PV-positive INs did not express GFP (n = 10 mice; 467 and 807 SST and PV INs, respectively, Fig. 1*A,B*). Consistent with the previous description of this mouse line (Ma et al., 2006), we also observed a population of GFP-positive non-neuronal cells presenting small soma area (< 40 μm^2). These non-neuronal cells were exclusively detectable after immunostaining against GFP (Fig. 1*A*), but were undetectable during electrophysiological recordings in brain slices.

In another series of experiments, several GFP-expressing neurons were filled with biocytin during whole-cell recordings and their morphology was traced to assess somato-dendritic and axonal morphology. Axons of L2/3 GFP-expressing neurons were systematically oriented towards superficial layers and consistently reached L1 where they were profusely branched (red tracing in Fig. 1*C*;

p=4.4E^{-4}, One-way ANOVA followed by Bonferroni post-hoc test, F=7.4716, n=10 reconstructed GFP-positive neurons). Conversely, GFP-expressing neurons dendrites were mostly located in L2/3 without reaching L1 (blue tracing in Fig. 1*C-E*).

We then measured the excitability and passive properties of GFP-expressing neurons (n = 22) and compared their firing pattern with that of PV INs (n = 14), the most abundant and perhaps best characterized GABAergic neuronal subtype (Fig. 2*A,B*). As previously described, the majority of the GFP-positive cells in X98 mice displayed a characteristic sag in response to hyperpolarizing current injection and a highly adapting firing behavior when depolarizing currents triggered repetitive spiking (Fig 2B). Conversely, PV INs displayed fast-spiking, non-adapting pattern in response to depolarizing currents (adaptation index: 2.27 ± 0.17 and 1.07 ± 0.04 for GFP-expressing and PV INs, respectively; p=1.1E^{-5}, Mann-Whitney U test; Fig. 2*C-E*), more hyperpolarized resting membrane potential (V_m: -66 ± 1 and -71 ± 1 mV for GFP-expressing and PV INs, respectively; p=0.0017, unpaired T test) and lower input resistance (R_i: 189 ± 11 and 92 ± 10 MΩ for GFP-expressing and PV INs, respectively; p=8.1E^{-6}, Mann-Whitney U test; Fig. 2*B*).

We then assessed the biophysical and pharmacological traits of synaptic transmission that distinguish x98 MCs from other INs. We analyzed unitary glutamatergic, excitatory and GABAergic, inhibitory currents (uEPSCs and uIPSCs, respectively) onto and from X98 MCs in X98 MC-PN connected pairs. One hallmark of MC connectivity is the strongly facilitating glutamatergic synaptic responses evoked upon PN action potentials (Wang et al., 2004; Kapfer et al., 2007; Silberberg and Markram, 2007). Accordingly, we found that unitary excitatory inputs from PNs to X98 MCs were invariably facilitating while uEPSCs onto PV INs were depressing (paired pulse ratio: 1.8 ± 0.2 for GFP-expressing neurons and 0.4 ± 0.1 for PV INs; p=1.8E^{-6}, Mann-Whitney U test; Fig 1 F-H). Finally, we analyzed the kinetics of uIPSCs elicited by X98 MCs and PV-cells in L2/3 PNs. We found that uIPSCs evoked from X98 MCs had significantly slower rise times as compared to PV INs (Rise time: 1.89 ± 0.25 ms for GFP-expressing neurons and 0.57 ± 0.02 for PV INs; p=2.2E^{-5}, unpaired T test; Fig. 1*I*), consistent with characteristic MC-mediated dendritic uIPSCs.

Altogether, these results indicate that GFP-expressing neurons in L2/3 of the somatosensory cortex of X98 mice exhibit morpho-functional features of L2/3 MCs (Wang et al., 2004; Gouwens et al., 2020). GFP-positive neurons in X98 mice (X98 MCs) can be readily distinguished from the most abundant GABAergic PV INs.

X98 Martinotti Cells display target-specific synaptic properties

In addition to PNs, SST INs were shown to contact other inhibitory neurons of the cortical microcircuits including VIP, PV and L1 INs (Ma et al., 2006; Pfeffer et al., 2013; Tremblay et al., 2016; Cao et al., 2020). However, it remains unknown whether this is true for X98 MCs and whether these connections exhibit the biophysical and pharmacological properties observed at the inhibitory synapses between X98 MCs and PNs. In order to address this question, we first explored the presence of synaptic markers of inhibitory synaptic contacts from X98 MCs onto other elements of the cortical microcircuit. We found that L2/3 GFP-positive axonal varicosities were juxtaposed to gephyrin-positive puncta located in PV- and VIP-positive somas (Fig. 3*A,D*) and co-expressed vGAT (Fig. 3*B,E*, suggesting axo-somatic synaptic contacts of X98-MCs onto PV and VIP INs. Axon terminals co-expressing GFP and vGAT were also juxtaposed to gephyrin-positive puncta around the somas of L1 INs (Fig. 3*G, H*). Conversely, PV and vGAT labelling onto L2/3 PNs showed characteristic basket structures devoid of GFP-positive axon terminals from X98 MCs (white asterisk; Fig. 3*J,K*). In order to quantify the incidence of X98 MCs axo-somatic synaptic contacts onto the different neuronal types we counted the number of GFP- and vGAT-positive puncta juxtaposed to the somas of L2/3 PV-positive, L2/3 VIP-positive, L2/3 NeuN-positive, putative PNs, and L1 NeuN-positive cells. We found that X98 MCs make on average 0.94 +/- 0.18 synaptic contacts onto PV INs (n = 47 cells, 4 mice); 2.04 +/- 0.35 onto VIP INs (n = 28 cells, 4 mice); 2.03 +/- 0.35 onto L1 INs (n = 34 cells, 3 mice) and 0.29 +/- 0.08 onto L2/3 NeuN-positive cells (n = 42 cells, 3 mice, Fig. 3*C,F,I,L*). Altogether, these results

suggest that X98 MCs make direct, axo-somatic synaptic contacts onto PV-, VIP- and L1 INs but not onto PNs.

We then studied the functional characteristics of the synaptic contacts formed by X98 MCs with other cortical INs. We performed dual patch recordings in brain slices and evoked uIPSCs from specific synapses formed by X98 MCs. To measure and compare evoked uIPSCs from pairs between MCs and other INs, we used brain slices containing differently labeled IN subtypes. For X98 MC-PV synapses, we crossed X98 mice with *Pvalb*-tdTomato mice. For MC-L1 synapses, we used X98 mice and L1 INs were identified by their localization in L1. Finally, to record uIPSCs from MC-VIP cell pairs we crossed VIPcre with X98 mice. Mouse pups (P1-3) were then subjected to intracerebral injections of flexed AAV particles coding for the red fluorescent protein tdTomato. We could thus obtain mice, in which MCs and VIP cells were simultaneously labeled with GFP and tdTomato, respectively.

GABAergic synapses formed by MCs to PNs were slow due, at least in part, to their distal dendritic location and consequent electrotonic filtering (Rall, 1967). To further explore whether synaptic contacts made by X98 MCs onto other circuit elements followed a similar pattern, we compared amplitudes and kinetics of uIPSCs elicited by X98 MCs onto PNs, PV-, L1- and VIP-INs (Fig. 4A-F). Rise time (Rt) of X98 MC-PN uIPSCs were significantly slower than those recorded from X98 MC-PV, X98 MC-L1 and X98 MC-VIP-IN pairs (1.89 ± 0.25; 0.73 ± 0.10; 0.63 ± 0.13; 0.80 ± 0.15 ms, respectively; $p=1.5E^{-4}$, one-way ANOVA; n = 10, 7, 5, 6, respectively; Fig. 4*F*). Rise times of uIPSCs recorded from connected pairs between X98 MCs and PV, VIP and L1 INs were not significantly different (one-way ANOVA followed by Bonferroni post hoc test; Fig. 4*E*). Amplitudes of evoked uIPSCs were also variable between and within connected pairs (Fig. 4*F*). uIPSC amplitudes were consistently larger in X98 MC-IN than in X98 MC-PN synapses (uIPSC amplitudes: 10 ± 1; 36 ± 4; 72 ± 32; 172 ± 70 pA; X98 MC-PN, -PV, L1 and VIP INs, respectively; $p = 6.36E^{-4}$; Kruskal Wallis followed by Mann-Withney with Bonferroni's correction; n = 10, 7, 5, 6 synapses, respectively; Fig. 4*E*).

We found significant connectivity rates between X98 MCs and PV INs (13 connected out of 85 recorded pairs), between X98 MCs and L1 INs (11 connected out of 80 recorded pairs) and between X98 MCs and VIP INs (9 connected out of 45 recorded pairs; Fig. 4*G*). Yet, the connectivity rate between X98 MCs and these IN types was much lower than functional connections with PNs (30 connected out of 57 recorded pairs; Fig. 4*G*). Conversely, we did not find functional synaptic transmission between X98 MCs (0 out of 10, connected/recorded pairs; Fig 4 G).

Altogether, these results indicate that L2/3 X98 MCs preferentially contact PNs, to a lesser, albeit non-negligible, extent PV, VIP and L1 INs, and avoid connecting between themselves. X98 MC-dendrite targeting is specific for connections with PNs.

We then analyzed STP at all unitary connections made by X98 MCs with different postsynaptic targets (Fig. 5*A,B*), in response to trains of 5 action potentials at 50 Hz. We found that STP profiles depended on the postsynaptic target. Indeed, normalized amplitudes of uIPSCs at X98 MC-PN and X98 X98 MC-L1 IN pairs were strongly depressing. In contrast, X98 MC-PV uIPSCs did not vary during the stimulus train, and X98 MC-VIP synapse exhibited a significant facilitating profile (Fig. 5*A-C*). When compared with X98 MC-PN connections, STP at X98 MC-L1 IN synapses were not significantly different. However, STP of X98 MC-PV and X98 MC–VIP IN synapses was significantly different than X98 MC-PN connections (repeated measures, two-way ANOVA followed by Bonferroni post hoc test; $F=24.1516$, $p=7.34E^{-5}$, n=5, 7, 5 and 7 synapses for X98 MC-VIP, -PV, -L1 and –PN, respectively; Fig. 3*B,C*).

Although we observed variability within the different synaptic contact types analyzed, altogether this results suggest that STP at X98 MC-synapses exhibit target specificity reflecting synapse-specific pre- and postsynaptic mechanisms.

α5-GABA$_A$Rs define X98 MC-PN synapses in L2/3 of mouse somatosensory cortex

Synaptic transmission between MCs and PNs was shown to be mediated by $GABA_A$Rs containing the α5 subunit in the rat somatosensory cortex (Ali and Thomson, 2008), in the mouse prefrontal cortex (Zorrilla de San Martin et al., 2020) and in the SST-expressing, Oriens Lacunosum-Moleculare (OL-M) INs to PN synapse (Schulz et al., 2018). Furthermore, in the rat somatosensory cortex, PV-IN-mediated PN perisomatic inhibition is sensitive to zolpidem (100 nM), a positive allosteric modulator, which at this concentration, is known to specifically bind to the benzodiazepine site of α1-containing and, less efficiently, α2- and α3-containing $GABA_A$ receptors (Korpi et al., 2002; Möhler, 2002; Bacci et al., 2003). In order to validate these results in the mouse somatosensory cortex we tested the effects of α5IA, a negative allosteric modulator (NAM) specific for α5-$GABA_A$Rs (Dawson et al., 2006), and zolpidem on both X98 MC-mediated PN dendritic inhibition and PV-IN-mediated PN perisomatic inhibition (Fig. 6*A*). PV-PN uIPSC weighted decay time constant ($\tau_{d,w}$) was significantly increased by zolpidem (control: 9.0 ± 1.3 ms; zolpidem: 11.2 ± 0.7 ms, n=6 pairs, p=0.014, Paired t-test; left panel, Fig 6*B*). In contrast, PV-PN uIPSCs amplitude was unaffected by α5IA (control: 63 ± 22 pA; α5IA: 65 ± 20 pA, n=6 pairs, p=0.7294, Paired t-test; right panel, Fig. 6*B*). The amplitude of uIPSCs elicited from X98 MCs was highly sensitive to α5IA (control: 177 ± 44 pA; α5IA: 104 ± 23 pA, n=11 pairs; p=0.003, Wilcoxon Signed-Ranks test; right panel, Fig 6*C*), and zolpidem did not affect the weighted decay time constant of the X98 MC-PN uIPSCs (control: 8.2 ± 1.2 ms; zolpidem: 9.1 ± 0.9, n=6 pairs, p=0.173, paired T test, , left panel, Fig 6*C*). α5IA is a partial NAM displaying ~40% efficacy, thus not providing a complete blockade of α5-$GABA_A$Rs (Dawson et al., 2006). Accordingly, after incubation with α5IA, the remaining X98 MC-PN uIPSC amplitude was near 60% (65.7% ± 5.4%; Fig. 6*C*). This suggests that unitary synaptic responses from X98 MCs to PNs are fully mediated by α5-$GABA_A$Rs.

α5-$GABA_A$Rs have been hypothesized to be extrasynaptic, mainly mediating tonic inhibition (Caraiscos et al., 2004). However, there is growing evidence that α5-$GABA_A$R are also involved in dendritic inhibition at specific synapses made by MCs in the cortex and by OLM INs in the hippocampus (Ali and Thomson, 2008; Schulz et al., 2018; Zorrilla De San Martin et al., 2020). It is

possible that sensitivity of uIPSCs to α5IA could be partially or fully due to activation of extrasynaptic $GABA_A$Rs due to GABA spillover, induced by AP-evoked synaptic transmission. To further study the role of synaptic α5-$GABA_A$Rs, we measured spontaneous inhibitory postsynaptic currents (sIPSCs) recorded from PNs (Fig 6 D-F). Because quantal, AP-independent synaptic events make up a large fraction of sIPSCs, these are less likely shaped by activation of extrasynaptic receptors. To separate putative dendritic and perisomatic events, we sorted sIPSCs into two groups based on their rise-times (Fig 6 D-F). We considered the events with rise times larger than 1.8 ms as 'slow', whereas those with rise-times smaller than 1.8 ms were defined as 'fast', based on the average rise-time obtained at connected X98 MC-PN pairs (Figs. 1I; 2C-E). The amplitudes of slow sIPSCs were significantly reduced after 10 minutes incubation with 100 nM α5IA (control: 31 ± 2 pA, α5IA: 28 ± 1 pA, n=11 cells, p=0.03, Wilcoxon Signed-Ranks test; Fig. 6*E*). Conversely, the same concentration of α5IA did not affect fast sIPSCs amplitude (control: 38 ± 2 pA, α5IA: 36 ± 2 pA; n=11 cells, p=0.3636, Wilcoxon Signed-Ranks test; Fig 6 F). This result indicates that fast, perisomatic events are generated by other INs types, not using α5-$GABA_A$Rs.

Altogether, these results indicate that synapses formed by dendrite-targeting X98 MCs onto PNs, specifically express α5-$GABA_A$Rs whereas PV-PN synapses express α1-$GABA_A$Rs.

X98 MCs inhibit PNs, but not other INs, through α5-$GABA_A$Rs.

In the previous sections, we showed that X98 MCs make synaptic contacts exhibiting target-specific biophysical and physiological properties. We also showed that, among the inhibitory inputs received by PNs, those originating from X98 MCs are distinguished by their sensitivity to α5IA. We therefore tested whether postsynaptic expression of α5-$GABA_A$Rs is a trait shared by all synaptic contacts made by X98 MCs or it is specific for synaptic contacts that X98 MCs form on PN dendrites. To address this question, we measured unitary GABAergic synaptic transmission between X98 MCs and other INs and tested their sensitivity to α5IA. We found that uIPSC amplitudes elicited by X98

MCs and recorded in PV INs (control: 31 ± 4 pA, α5IA: 35 ± 6 pA, n=11 pairs, p=0.3757, paired t test) , L1 INs (control: 83 ± 32 pA, α5IA: 102 ± 29 pA, n=5 pairs, p=0.3757, paired t test) and VIP INs (control: 178 ± 100 pA, α5IA: 118 ± 52 pA, n=4 pairs, p=0.7432, Wilcoxon signed ranks test) were not sensitive to α5IA (Fig. 7*B-C*).

In the hippocampus, SST-positive, OL-M INs receive α5-mediated inhibition from VIP INs (Magnin et al., 2019). Since VIP-MC synapses represent an important disinhibitory circuit in the cortex as well, we tested whether α5-$GABA_A$Rs mediate inhibitory inputs from VIP INs also in the mouse somatosensory cortex. To address this question, we crossed VIP-cre with X98 mice (VIP-cre::X98 mice). Since dual whole-cell recordings produced a very low yield (3 connected out of 45 recorded pairs), we expressed the light-sensitive opsin ChR2 via injection of flexed-ChR2 AAV particles in the barrel cortex of 1-3 days old VIP-cre::X98 pups. We activated VIP INs and recorded light-evoked IPSCs in X98 MCs. We found that inhibitory responses originating from VIP cells were not sensitive to α5IA (control: 170 ± 46 pA, α5IA: 166 ± 52 pA, n=7, p=0.7432, Wilcoxon signed ranks test; Fig 7 B).

Overall, these results indicate that GABAergic inhibition involving X98 MCs uses α5-$GABA_A$Rs exclusively at synapses formed with PN distal dendrites and not for other X98 MC-targets within cortical circuits. Thus, the characteristic slow kinetics of uIPSCs, the distal dendritic targeting and the synaptic expression of α5-$GABA_A$Rs represent unique molecular and cellular signatures of X98 MC-PN synapses.

Tonic inhibition is mediated by α5-$GABA_A$Rs in PN, but not in X98 MC nor PV-IN.

α5-$GABA_A$Rs have been largely associated to tonic inhibition due to extrasynaptic immunoreactivity in cell culture (Loebrich et al., 2006; Serwanski et al., 2006), hippocampus and cortex (Serwanski et al., 2006) and amygdala (Botta et al., 2015) and the lack of tonic inhibitory current in hippocampal PNs of α5 knock-out mice (Caraiscos et al., 2004).

Thus, we pre-incubated slices with aCSF or aCSF + 100 nM α5IA during at least 10 minutes and then quantified the difference in holding current amplitude (ΔI_{hold}) before and after bath application of 1 µM gabazine (Fig. 8). Pre-incubation with 100 nM α5IA significantly reduced GABAergic ΔI_{hold} in PNs as compared to slices preincubated in aCSF only (aCSF: 51 ± 1 pA, n=16; α5IA: 29 ± 7 pA, n=23, p=0.0244, unpaired t test; Fig. 8*A,B*). Conversely, incubation with α5IA failed to produce any significant change in tonic current recorded from X98 MCs (aCSF: 16 ± 5 pA, n=9; α5IA: 23 ± 6 pA, n=14, p=0.3330, unpaired t test; Fig. 8*C,D*) nor PV INs (aCSF: 33 ± 10 pA, n=9; α5IA: 24 ± 5 pA, n=14, p=0.6591, unpaired t test; Fig. 8*E,F*), showing that tonic inhibition is mediated by α5-$GABA_A$Rs exclusively in PNs.

Altogether, these results indicate that α5-$GABA_A$Rs are selectively expressed by PNs and they mediate both tonic and dendritic, phasic synaptic inhibition.

Discussion

In this study, we explored physiological aspects of different inhibitory synaptic connections made by a subset of SST-positive INs in the L2/3 of the mouse somatosensory cortex, the X98 MCs. We show that inhibitory synapses made by X98 MCs display biophysical, morphological and pharmacological properties that are specific in distinct postsynaptic partners. We found that the most extensively contacted cells are PNs. However, also PV, VIP and L1 inhibitory INs also receive significant inhibition from X98 MCs. Notably, we showed that the X98 MC-PN synapse is distinguished by two unique features: slow kinetics and expression of the α5-$GABA_A$R. Finally, we showed that α5-$GABA_A$Rs contribute to tonic inhibition of PNs but not of other INs, confirming the specific involvement of this receptor in PN dendritic inhibition.

SST-cre mouse lines are widely used to study the functional role of SST-expressing INs by manipulating and recording their activity, using cre-driven expression of light-sensitive opsins or genetically encoded Ca^{2+} sensors (Taniguchi et al., 2011). Despite its extensive use, the SST-cre

mouse line affects all INs expressing SST. Yet, SST-positive neurons encompass a highly heterogeneous group of inhibitory neurons that display diverse molecular profile, morphology, spiking patterns and connectivity (Halabisky et al., 2006; Ma et al., 2006; McGarry et al., 2010; Riedemann et al., 2016; Naka et al., 2019; Gouwens et al., 2020; Zhou et al., 2020; Bugeon et al., 2022). Here we provide evidence that GFP-expressing neurons in the somatosensory cortex of young (P18-25) X98 mice account for 68% of SST-expressing INs and exhibit morpho-functional properties of L2/3 MCs, (Wang et al., 2004; Kapfer et al., 2007; Silberberg and Markram, 2007; Tremblay et al., 2016; Gouwens et al., 2020). Previous estimates indicate that the subpopulation of GFP-expressing neurons from X98 adult mice represents a specific subset of GABAergic INs, accounting for 16% (all layers) or 13% (L2/3) of all SST neurons (Ma et al., 2006). This discrepancy could be due to developmental differences between the range of ages used in this study and that of the original quantification (2-3 months after birth; Ma et al. 2006), or simply to differences in the sample size used in this and the original study. Since this mouse line is based on the GAD promoter and a random insertion into the mouse genome (Ma et al., 2006), we cannot rule out the possibility of other subtypes of MCs that do not express GFP and thus were not included in our experiments. However, our results indicate that GFP-positive neurons encompass a large majority of SST-expressing INs, which belong to the broad class of SST-expressing MCs. Determining whether GFP-positive neurons in X98 mice comprehensively capture a specific MC subclass will require RNAseq analysis from GFP-expressing neurons (Gouwens et al., 2020; Bugeon et al., 2022).

Even though X98 MCs extensively inhibit PNs via α5-$GABA_A$Rs, they also contact other elements of the cortical microcircuits, and, in addition, they are targeted by VIP-expressing INs (Pfeffer et al., 2013; Kepecs and Fishell, 2014; Tremblay et al., 2016; Walker et al., 2016). We found that X98 MCs contact PV- VIP- and L1-INs at a reduced connectivity rate, as compared to X98 MC-PN connections. Moreover, GABAergic synapses from X98 MCs onto other INs and those inhibiting X98 MCs from VIP-INs do not use α5-$GABA_A$Rs.

MCs were hypothesized to provide a non-specific 'blanket' of inhibition to PNs (Fino and Yuste, 2011; Fino et al., 2013; Karnani et al., 2016). Accordingly, we found a relatively high connectivity rate between X98 MCs and L2/3 PNs, consistent with the prominent X98 MC axonal plexus innervating L1. In addition to PN dendrites, despite at lower rate, X98 MCs contact also L1-INs, which exert slow feed-forward inhibition on PN dendrites during the encoding of context-rich, top-down information from higher order thalamus and cortices (Letzkus et al., 2011; Abs et al., 2018). X98 MC-L1 IN connectivity was relatively low. However, we could have underestimated X98 MC-L1 IN connectivity, as we did not discriminate different L1 IN subclasses. Indeed, SST INs have been reported to privilege NDNF-positive INs of L1 (Abs et al., 2018).

Importantly, dendritic inhibition seems to be a specific feature of X98 MC-PN connections, as uIPSC rise times measured on other X98 MC targets (INs) had fast (<1 ms) kinetics similar to the known PV-PN perisomatic responses. In agreement with this view, we failed to find evidence of direct contact between X98 MC axons on the perisomatic region of PNs. Conversely, we found X98 MC VGAT-positive boutons juxtaposed to the gephyrin-positive puncta onto the perisomatic region of PV, VIP and L1 INs. This is consistent with the fast, non-filtered, IPSCs observed in somatic whole-cell recordings and in line with a previous report showing that inhibitory contacts onto PV INs are preferentially located in the proximal dendrites and soma while excitatory inputs are located in distal dendrites (Kameda et al., 2012).

Use-dependent short-term facilitation or depression of synaptic responses has been traditionally linked to specific synaptic mechanisms identifying diverse cell types with specific pre- and postsynaptic biophysical properties, such as low or high release probability, respectively (Jackman and Regehr, 2017). Importantly, frequency-dependent bidirectional STP is a powerful synaptic tool to provide distinct cell types with a specific strategy to transfer information about presynaptic spike trains. We found that GABAergic synapses from X98 MCs exhibit target-cell-specific facilitation and depression. Target-cell-specific STP and release probability, originating from the same cell type, was described at glutamatergic synapses from PNs recruiting different IN subtypes in the neocortex and

hippocampus (Reyes et al., 1998). Our finding indicates that single-axon, target-specific bidirectional STP occurs also at GABAergic synapses. Intriguingly, synapses made in L1 (with either PN distal dendrites or sparse INs) are depressing, whereas, inhibitory connection that the same cells make onto their targets in L2/3 (PV and VIP cells) are either unvarying or strongly facilitating. It will be interesting to reveal the molecular and synaptic mechanisms underlying the target-specificity of GABAergic synapses originating from the same X98 MC onto different elements of the cortical circuit. Interestingly, STP of unitary inhibitory-to-inhibitory synapses from PV and SST cells was shown to be determined by the identity of the presynaptic interneuron (Ma et al., 2012). Target cell type-dependent variability in presynaptic properties increases the computational power of neuronal networks. It will be therefore fundamental to understand the functional role of such a target-specific regulation of inhibitory synaptic efficacy.

X98 MCs exhibit differential inhibitory strategies depending on the postsynaptic cell type: they modulate input onto PNs and they likely control, at least in part, the output activity of other INs. Therefore, inhibitory circuits formed by X98 MCs seem to exhibit a more complex architecture and function than previously hypothesized as provider of a mere blanket of inhibition (Fino and Yuste, 2011).

In addition to the strong preference for distal apical dendrites, X98 MCs display another PN-specific synaptic feature, as they use α5-$GABA_A$Rs for synaptic dendritic inhibition. Indeed, GABAergic synapses from X98 MCs to other INs are perisomatic and do not use α5-$GABA_A$Rs. In fact, lack of α5IA effects on tonic inhibition on PV and X98 MCs suggest that these major IN subtypes do not express this $GABA_A$R α subunit. This is in line with gene expression results in different cortical neuron subtypes, indicating PNs as majorly expressing α5-$GABA_A$Rs (Hu et al., 2018). Transcriptomics analysis of different $GABA_A$R subunits in specific cortical interneuron subclasses indicates relative low expression of *Gabra5* in all interneuron subclasses as compared to *Gabra1* and *Gabra2* (Winterer et al., 2019). Yet, we cannot exclude that other IN subtypes might use α5-$GABA_A$Rs at their inhibitory synapses with PNs and other INs. Interestingly, it has been recently reported that

hippocampal Oriens-Lacunosum Moleculare INs also express, α5-$GABA_A$Rs at synapses originating at VIP INs (Magnin et al., 2019). Yet, we did not find evidence of α5IA effect on VIP-IN-evoked IPSCs in X98 MCs of the barrel cortex, suggesting that cortical MCs differ from their hippocampal counterparts. The α5 subunit is much more strongly expressed in the hippocampus than in the neocortex (Lingford-Hughes et al., 2002). Therefore, it will be interesting to reveal whether α5 has different circuit-specificity and/or plays a different role in these two areas. Likewise, it remains to be tested whether α5-$GABA_A$Rs are also expressed by other subtypes of inhibitory neurons. Our results on L1-INs suggest that X98 MCs do not use α5-$GABA_A$Rs at these synapses. However, L1 is populated by a heterogeneous IN population (Schuman et al., 2019) and, since we did not use specific mouse lines to target distinct cell types, our data may have been collected from a relatively heterogeneous interneuron group. Overall, our results are consistent with a previous report indicating that synapses from SST+ INs to other non-specified INs are insensitive to α5-IA (Cao et al., 2020) .

In addition to dendritic filtering, X98 MC-PN synaptic responses might be slow due to the specific properties of the α5-subunit itself, which is exclusively expressed at this synapse. The slow kinetics and the rectification of α5-$GABA_A$Rs match the biophysical properties of NMDARs, which govern Ca^{2+} signaling and dendritic computation in PNs (Branco and Häusser, 2010; Tran-Van-Minh et al., 2015; Schulz et al., 2018). Dendritic patch would be necessary to test this hypothesis, although the high series resistance typical of dendritic patch recordings might prevent an accurate analysis of fast currents.

α5-$GABA_A$Rs have been proposed to mediate tonic inhibition due to their sensitivity to nanomolar concentrations of GABA, their non-desensitizing properties and the lack of evidence supporting its implication in synaptic transmission (Caraiscos et al., 2004). However, knock down of radixin, the extrasynaptic scaffolding protein associated to α5-$GABA_A$Rs did not produce any effect on GABA evoked current, suggesting that extrasynaptic α5-$GABA_A$Rs might not be functional (Loebrich et al., 2006). Furthermore, the participation of α5-$GABA_A$Rs in phasic synaptic inhibition has been recently demonstrated in different brain structures, namely the rat somatosensory cortex (Ali and Thomson,

637 2008), mouse hippocampus (Schulz et al., 2018; Lodge et al., 2021) and mouse prefrontal cortex
638 (Zorrilla De San Martin et al., 2020). Even for action potential-dependent unitary responses between
639 X98 MCs and PNs, it is possible that GABA could spill over to peri- or extrasynaptic $GABA_A$Rs
640 containing α5. If this were the case, we would not have detected significant effects on quantal
641 events, which reflect mostly purely synaptic activation of $GABA_A$Rs. Importantly, we recorded sIPSCs
642 from the soma of L2/3 PNs and found that only slow sIPSCs were sensitive to α5IA, whereas fast
643 perisomatic inhibitory events were unaffected. Our results on sIPSCs corroborate the synaptic
644 localization of α5-$GABA_A$Rs. Indeed, at our extracellular K^+ concentrations, sIPSCs are dominated by
645 AP independent miniature events. The blockade of X98 MC-PN uIPSCs, slow sIPSCs and tonic
646 inhibition was not total but it was in all cases maximal, taking into account the actual efficacy (~40%)
647 of α5IA (Sternfeld et al., 2004; Atack, 2010).

648 Therefore, the most parsimonious interpretation of our pharmacological experiments is that α5-
649 $GABA_A$Rs are prominently expressed at synaptic sites of dendritic X98 MC-PN connections and are
650 responsible for dendritic inhibition from this specific GABAergic neuron type. In fact, the α5-
651 mediated tonic currents could be the direct activation by ambient GABA of high affinity synaptic, and
652 not necessarily extrasynaptic receptors. However, we cannot exclude that both synaptic and
653 extrasynaptic α5-$GABA_A$Rs receptors exist and dynamically interact (see Hausrat et al., 2015)

654 The specific expression of the α5 $GABA_A$R subunit in PNs is particularly interesting in light of its
655 involvement in cognitive processes. Mice lacking the *Gabra5* gene, encoding for the α5 subunit of
656 the $GABA_A$R, show enhanced performance in cognitive tasks (Collinson et al., 2002). This evidence, in
657 addition to the high α5-$GABA_A$Rs expression in the mouse prefrontal cortex and hippocampus
658 (Fritschy and Mohler, 1995) led to propose novel potential pro-cognitive pharmacological strategies
659 in several brain disorders, such as intellectual disability in Down syndrome, memory deficits and
660 depression (Braudeau et al., 2011; Martínez-Cué et al., 2013; Duchon et al., 2019; Zorrilla De San
661 Martin et al., 2020; Zurek et al., 2014; Zanos et al., 2017). Specific negative modulation of these
662 receptors would facilitate cognition avoiding anxiogenic and pro-convulsive effects of wide spectrum

663 $GABA_ARs$ antagonists due to the restricted expression of the α5 subunit to this specific inhibitory
664 circuit formed by MCs.

665

666 ## References

667 Abs E, Poorthuis RB, Apelblat D, Muhammad K, Pardi MB, Enke L, Kushinsky D, Pu D-L, Eizinger MF,
668 Conzelmann K-K, Spiegel I, Letzkus JJ (2018) Learning-Related Plasticity in Dendrite-Targeting
669 Layer 1 Interneurons. Neuron:1–16.

670 Adesnik H, Bruns W, Taniguchi H, Huang ZJ, Scanziani M (2012) A neural circuit for spatial summation
671 in visual cortex. Nature 490:226–230.

672 Adesnik H, Scanziani M (2010) Lateral competition for cortical space by layer-specific horizontal
673 circuits. Nature 464:1155–1160.

674 Ali AB, Thomson AM (2008) Synaptic α5 subunit-containing GABAA receptors mediate ipsps elicited
675 by dendrite-preferring cells in rat neocortex. Cereb Cortex 18:1260–1271.

676 Atack JR (2010) Preclinical and clinical pharmacology of the GABAA receptor α5 subtype-selective
677 inverse agonist α5IA. Pharmacol Ther 125:11–26.

678 Bacci A, Rudolph U, Huguenard JR, Prince DA (2003) Major Differences in Inhibitory Synaptic
679 Transmission onto Two Neocortical Interneuron Subclasses. J Neurosci 23:9664–9674.

680 Bartos M, Vida I, Jonas P (2007) Synaptic mechanisms of synchronized gamma oscillations in
681 inhibitory interneuron networks. Nat Rev Neurosci 8:45–56.

682 Berger TK, Perin R, Silberberg G, Markram H (2009) Frequency-dependent disynaptic inhibition in the
683 pyramidal network: a ubiquitous pathway in the developing rat neocortex. J Physiol 587:5411–
684 5425.

685 Botta P, Demmou L, Kasugai Y, Markovic M, Xu C, Fadok JP, Lu T, Poe MM, Xu L, Cook JM, Rudolph U,

686 Sah P, Ferraguti F, Lüthi A (2015) Regulating anxiety with extrasynaptic inhibition. Nat Neurosci
687 18:1493–1500.

688 Branco T, Häusser M (2010) The single dendritic branch as a fundamental functional unit in the
689 nervous system. Curr Opin Neurobiol 20:494–502.

690 Braudeau J, Delatour B, Duchon A, Pereira PL, Dauphinot L, de Chaumont F, Olivo-Marin J-C, Dodd R,
691 Hérault Y, Potier M-C (2011) Specific targeting of the GABA-A receptor {alpha}5 subtype by a
692 selective inverse agonist restores cognitive deficits in Down syndrome mice. J Psychopharmacol
693 25:1030–1042.

694 Bugeon S, Duffield J, Dipoppa M, Ritoux A, Prankerd I, Nicoloutsopoulos D, Orme D, Shinn M, Peng H,
695 Forrest H, Viduolyte A, Reddy CB, Isogai Y, Carandini M, Harris KD. A transcriptomic axis
696 predicts state modulation of cortical interneurons. Nature. 2022 Jul;607(7918):330-338.
697 Erratum in: Nature. 2022 Aug 25.

698 Buzsáki G (2010) Neural Syntax: Cell Assemblies, Synapsembles, and Readers. Neuron 68:362–385.

699 Buzsáki G, Wang X-J (2012) Mechanisms of Gamma Oscillations. Annu Rev Neurosci 35:203–225.

700 Cao JW, Guan W, Yu YC, Fu Y. Synaptic Transmission from Somatostatin-expressing Interneurons to
701 Excitatory Neurons Mediated by α5-subunit-containing GABAA Receptors in the Developing
702 Visual Cortex. Neuroscience. 2020 Nov 21;449:147-156.

703 Caraiscos VB, Elliott EM, You-Ten KE, Cheng VY, Belelli D, Newell JG, Jackson MF, Lambert JJ, Rosahl
704 TW, Wafford K a, MacDonald JF, Orser B a (2004) Tonic inhibition in mouse hippocampal CA1
705 pyramidal neurons is mediated by alpha5 subunit-containing gamma-aminobutyric acid type A
706 receptors. Proc Natl Acad Sci U S A 101:3662–3667.

707 Clem RL, Cummings KA (2020) Prefrontal somatostatin interneurons encode fear memory. Nat
708 Neurosci 23:p61, 14 p.

709 Collinson N, Kuenzi FM, Jarolimek W, Maubach K a, Cothliff R, Sur C, Smith A, Otu FM, Howell O,

710 Atack JR, McKernan RM, Seabrook GR, Dawson GR, Whiting PJ, Rosahl TW (2002) Enhanced
711 learning and memory and altered GABAergic synaptic transmission in mice lacking the alpha 5
712 subunit of the GABAA receptor. J Neurosci 22:5572–5580.

713 Dawson GR, Maubach KA, Collinson N, Cobain M, Everitt BJ, MacLeod AM, Choudhury HI, McDonald
714 LM, Pillai G, Rycroft W, Smith AJ, Sternfeld F, Tattersall FD, Wafford KA, Reynolds DS, Seabrook
715 GR, Atack JR (2006) An inverse agonist selective for α5 subunit-containing GABA A receptors
716 enhances cognition. J Pharmacol Exp Ther 316:1335–1345.

717 Duchon A, Gruart A, Albac C, Delatour B, Zorrilla de San Martin J, Delgado-García JM, Hérault Y,
718 Potier MC (2019) Long-lasting correction of in vivo LTP and cognitive deficits of mice modelling
719 Down syndrome with an α5-selective GABAA inverse agonist. Br J Pharmacol 177:1106–1118.

720 Duncan CE, Webster MJ, Rothmond DA, Bahn S, Elashoff M, Shannon Weickert C (2010) Prefrontal
721 GABAA receptor α-subunit expression in normal postnatal human development and
722 schizophrenia. J Psychiatr Res 44:673–681.

723 Fino E, Packer AM, Yuste R (2013) The logic of inhibitory connectivity in the neocortex.
724 Neuroscientist 19:228–237.

725 Fino E, Yuste R (2011) Dense inhibitory connectivity in neocortex. Neuron 69:1188–1203.

726 Fritschy JM, Mohler H (1995) GABAA receptor heterogeneity in the adult rat brain: Differential
727 regional and cellular distribution of seven major subunits. J Comp Neurol 359:154–194.

728 Gill K, Grace A (2014) The Role of α5 GABAA Receptor Agonists in the Treatment of Cognitive Deficits
729 in Schizophrenia. Curr Pharm Des 20:5069–5076.

730 Goldberg EM, Jeong HY, Kruglikov I, Tremblay R, Lazarenko RM, Rudy B (2011) Rapid developmental
731 maturation of neocortical FS cell intrinsic excitability. Cereb Cortex 21:666–682.

732 Gouwens NW et al. (2020) Integrated Morphoelectric and Transcriptomic Classification of Cortical
733 GABAergic Cells. Cell 183:935-953.e19.

734 Halabisky B, Shen F, Huguenard JR, Prince DA (2006) Electrophysiological classification of
735 somatostatin-positive interneurons in mouse sensorimotor cortex. J Neurophysiol 96:834–845.

736 Hausrat TJ, Muhia M, Gerrow K, Thomas P, Hirdes W, Tsukita S, Heisler FF, Herich L, Dubroqua S,
737 Breiden P, Feldon J, Schwarz JR, Yee BK, Smart TG, Triller A, Kneussel M (2015) Radixin
738 regulates synaptic GABAA receptor density and is essential for reversal learning and short-term
739 memory. Nat Commun 6:6872.

740 Hilscher MM, Leão RN, Edwards SJ, Leão KE, Kullander K, Bacci A (2016) Chrna2-Martinotti Cells
741 Synchronize layer 5 type A Pyramidal Cells via Rebound Excitation. PLoS Biol 15.

742 Hu X, Rocco BR, Fee C, Sibille E (2018) Cell Type-Specific Gene Expression of Alpha 5 Subunit-
743 Containing Gamma-Aminobutyric Acid Subtype A Receptors in Human and Mouse Frontal
744 Cortex. Mol Neuropsychiatry 4:204–215.

745 Isaacson JS, Scanziani M (2011) How inhibition shapes cortical activity. Neuron 72:231–243.

746 Jackman SL, Regehr WG (2017) The Mechanisms and Functions of Synaptic Facilitation. Neuron
747 94:447–464.

748 Jiang X, Shen S, Cadwell CR, Berens P, Sinz F, Ecker AS, Patel S, Tolias AS (2015) Principles of
749 connectivity among morphologically defined cell types in adult neocortex. Science (80-)
750 350:139–148.

751 Kaiser T, Ting JT, Monteiro P, Feng G (2016) Transgenic labeling of parvalbumin-expressing neurons
752 with tdTomato. Neuroscience 321:236–245.

753 Kameda H, Hioki H, Tanaka YH, Tanaka T, Sohn J, Sonomura T, Furuta T, Fujiyama F, Kaneko T (2012)
754 Parvalbumin-producing cortical interneurons receive inhibitory inputs on proximal portions and
755 cortical excitatory inputs on distal dendrites. Eur J Neurosci 35:838–854.

756 Kapfer C, Glickfeld LL, Atallah B V, Scanziani M (2007) Supralinear increase of recurrent inhibition
757 during sparse activity in the somatosensory cortex. Nat Neurosci 10:743–753.

758 Karnani MM, Jackson J, Ayzenshtat I, Sichani XH, Manoocheri K, Kim S, Yuste R (2016) Opening holes
759 in the blanket of inhibition: Localized lateral disinhibition by vip interneurons. J Neurosci
760 36:3471–3480.

761 Kepecs A, Fishell G (2014) Interneuron cell types are fit to function. Nature 505:318–326.

762 Korpi ER, Mihalek RM, Sinkkonen ST, Hauer B, Hevers W, Homanics GE, Sieghart W, Lüddens H
763 (2002) Altered receptor subtypes in the forebrain of GABAA receptor δ subunit-deficient mice:
764 Recruitment of γ2 subunits. Neuroscience 109:733–743.

765 Letzkus JJ, Wolff SBE, Meyer EMM, Tovote P, Courtin J, Herry C, Lüthi A (2011) A disinhibitory
766 microcircuit for associative fear learning in the auditory cortex. Nature 480:331–335.

767 Lingford-Hughes A, Hume SP, Feeney A, Hirani E, Osman S, Cunningham VJ, Pike VW, Brooks DJ, Nutt
768 DJ (2002) Imaging the GABA-benzodiazepine receptor subtype containing the alpha5-subunit in
769 vivo with [11C]Ro15 4513 positron emission tomography. J Cereb Blood Flow Metab 22:878–
770 889.

771 Lodge M, Hernandez MC, Schulz JM, Bischofberger J. Sparsification of AP firing in adult-born
772 hippocampal granule cells via voltage-dependent α5-GABAA receptors. Cell Rep. 2021 Oct
773 5;37(1):109768.

774 Loebrich S, Bä Hring R, Katsuno T, Tsukita S, Kneussel M (2006) Activated radixin is essential for
775 GABA A receptor a5 subunit anchoring at the actin cytoskeleton. EMBO J 25:987–999.

776 Lovett-Barron M, Turi GF, Kaifosh P, Lee PH, Bolze F, Sun X-HH, Nicoud J-FF, Zemelman B V, Sternson
777 SM, Losonczy A (2012) Regulation of neuronal input transformations by tunable dendritic
778 inhibition. Nat Neurosci 15:423–430.

779 Ma Y, Hu H, Agmon A (2012) Short-term plasticity of unitary inhibitory-to-inhibitory synapses
780 depends on the presynaptic interneuron subtype. J Neurosci 32:983–988.

781 Ma Y, Hu H, Berrebi AS, Mathers PH, Agmon A (2006) Distinct subtypes of somatostatin-containing

neocortical interneurons revealed in transgenic mice. J Neurosci 26:5069–5082.

Magnin E, Francavilla R, Amalyan S, Gervais E, David LS, Luo X, Topolnik L (2019) Input-specific synaptic location and function of the α5 GABA a receptor subunit in the mouse CA1 hippocampal neurons. J Neurosci 39:788–801.

Martínez-Cué C, Martinez P, Rueda N, Vidal R, Garcia S, Vidal V, Corrales A, Montero JA, Pazos A, Florez J, Gasser R, Thomas AW, Honer M, Knoflach F, Trejo JL, Wettstein JG, Hernandez M-C (2013) Reducing GABAA 5 Receptor-Mediated Inhibition Rescues Functional and Neuromorphological Deficits in a Mouse Model of Down Syndrome. J Neurosci 33:3953–3966.

McGarry LM, Packer AM, Fino E, Nikolenko V, Sippy T, Yuste R (2010) Quantitative classifi cation of somatostatin-positive neocortical interneurons identifi es three interneuron subtypes. Front Neural Circuits 4.

Möhler H (2002) Pathophysiological aspects of diversity in neuronal inhibition: A new benzodiazepine pharmacology. Dialogues Clin Neurosci 4:261–269.

Naka A, Veit J, Shababo B, Chance RK, Risso D, Stafford D, Snyder B, Egladyous A, Chu D, Sridharan S, Mossing DP, Paninski L, Ngai J, Adesnik H (2019) Complementary networks of cortical somatostatin interneurons enforce layer specific control. Elife 8:1–36.

Okaty BW, Miller MN, Sugino K, Hempel CM, Nelson SB (2009) Transcriptional and Electrophysiological Maturation of Neocortical Fast-Spiking GABAergic Interneurons. J Neurosci 29:7040–7052.

Paul A, Crow M, Raudales R, He M, Gillis J, Huang ZJ (2017) Transcriptional Architecture of Synaptic Communication Delineates GABAergic Neuron Identity. Cell 171:522-539.e20.

Pfeffer CK, Xue M, He M, Huang ZJ, Scanziani M (2013) Inhibition of inhibition in visual cortex: The logic of connections between molecularly distinct interneurons. Nat Neurosci 16:1068–1076.

Rall W (1967) Distinguishing theoretical synaptic potentials computed for different soma-dendritic

distributions of synaptic input. J Neurophysiol 30:1138–1168.

Reyes A, Lujan R, Rozov A, Burnashev N, Somogyi P, Sakmann B (1998) Target-cell-specific facilitation and depression in neocortical circuits. Nat Neurosci 1:279–285.

Riedemann T, Schmitz C, Sutor B (2016) Immunocytochemical heterogeneity of somatostatin-expressing GABAergic interneurons in layers II and III of the mouse cingulate cortex: A combined immunofluorescence/design-based stereologic study. J Comp Neurol 524:2281-2299

Scala F, Kobak D, Shan S, Bernaerts Y, Laturnus S, Cadwell CR, Hartmanis L, Froudarakis E, Castro JR, Tan ZH, Papadopoulos S, Patel SS, Sandberg R, Berens P, Jiang X, Tolias AS (2019) Layer 4 of mouse neocortex differs in cell types and circuit organization between sensory areas. Nat Commun 10:1–12.

Scheggia D, Manago F, Maltese F, Bruni S, Nigro M, Latuske P, Contarini G, Gomez-Gonzola M, Requie LM, Ferretti V, Castellani G, Mauro D, Bonavia A, Carmignoto G, Yizhar O, Papaleo F (2019) Somatostatin interneurons in the prefrontal cortex control affective state discrimination in mice. Nat Neurosci 23.

Schulz JM, Knoflach F, Hernandez M-C, Bischofberger J (2018) Dendrite-targeting interneurons control synaptic NMDA-receptor activation via nonlinear α5-GABAA receptors. Nat Commun 9:3576.

Schulz JM, Knoflach F, Hernandez MC, Bischofberger J (2019) Enhanced dendritic inhibition and impaired NMDAR activation in a mouse model of down syndrome. J Neurosci 39:5210–5221.

Schuman B, Machold RP, Hashikawa Y, Fuzik J, Fishell GJ, Rudy B (2019) Four unique interneuron populations reside in neocortical layer 1. J Neurosci 39:125–139.

Serwanski DR, Miralles CP, Christie SB, Mehta AK, Li X, Blas AL De (2006) Synaptic and non-synaptic localization of GABA A receptors containing the alpha5 subunit in the rat brain. J Comp Neurol Neurol 499:458–470.

Silberberg G, Markram H (2007) Disynaptic Inhibition between Neocortical Pyramidal Cells Mediated by Martinotti Cells. Neuron 53:735–746.

Sternfeld F, Carling RW, Jelley RA, Ladduwahetty T, Merchant KJ, Moore KW, Reeve AJ, Street LJ, O'Connor D, Sohal B, Atack JR, Cook S, Seabrook G, Wafford K, Tattersall FD, Collinson N, Dawson GR, Castro JL, MacLeod AM (2004) Selective, Orally Active γ-Aminobutyric AcidA α5 Receptor Inverse Agonists as Cognition Enhancers. J Med Chem 47:2176–2179.

Taniguchi H, He M, Wu P, Kim S, Paik R, Sugino K, Kvitsani D, Fu Y, Lu J, Lin Y, Miyoshi G, Shima Y, Fishell G, Nelson SB, Huang ZJ (2011) A Resource of Cre Driver Lines for Genetic Targeting of GABAergic Neurons in Cerebral Cortex. Neuron 71:995–1013.

Tran-Van-Minh A, Cazé RD, Abrahamsson T, Cathala L, Gutkin BS, DiGregorio DA (2015) Contribution of sublinear and supralinear dendritic integration to neuronal computations. Front Cell Neurosci 9:67.

Tremblay R, Lee S, Rudy B (2016) GABAergic Interneurons in the Neocortex: From Cellular Properties to Circuits. Neuron 91:260–292.

Ulrich D, Huguenard JR (1996) GABA(B) receptor-mediated responses in GABAergic projection neurones of rat nucleus reticularis thalami in vitro. J Physiol 493:845–854.

Walker F, Möck M, Feyerabend M, Guy J, Wagener RJ, Schubert D, Staiger JF, Witte M (2016) Parvalbumin-and vasoactive intestinal polypeptide-expressing neocortical interneurons impose differential inhibition on Martinotti cells. Nat Commun 7.

Wang Y, Toledo-Rodriguez M, Gupta A, Wu C, Silberberg G, Luo J, Markram H (2004) Anatomical, physiological and molecular properties of Martinotti cells in the somatosensory cortex of the juvenile rat. J Physiol 561:65–90.

Wilson NR, Runyan CA, Wang FL, Sur M (2012) Division and subtraction by distinct cortical inhibitory networks in vivo. Nature 488:343–348.

Winterer J, Lukacsovich D, Que L, Sartori AM, Luo W, Földy C (2019) Single-cell RNA-Seq characterization of anatomically identified OLM interneurons in different transgenic mouse lines. Eur J Neurosci 50:3750–3771.

Xu H, Jeong HY, Tremblay R, Rudy B (2013) Neocortical Somatostatin-Expressing GABAergic Interneurons Disinhibit the Thalamorecipient Layer 4. Neuron 77:155–167.

Yavorska I, Wehr M (2016) Somatostatin-expressing inhibitory interneurons in cortical circuits. Front Neural Circuits 10:76.

Zanos P, Nelson ME, Highland JN, Krimmel SR, Georgiou P, Gould TD, Thompson SM (2017) A negative allosteric modulator for α5 subunit- containing GABA receptors exerts a rapid and persistent antidepressant-like action without the side effects of the NMDA receptor antagonist ketamine in mice. eNeuro 4:285–301.

Zhou X, Mansori I, Fischer T, Witte M, Staiger JF (2020) Characterizing the morphology of somatostatin-expressing interneurons and their synaptic innervation pattern in the barrel cortex of the GFP-expressing inhibitory neurons mouse. J Comp Neurol 528:244-260

Zorrilla De San Martin J, Donato C, Peixoto J, Aguirre A, Choudhary V, De Stasi AM, Lourenço J, Potier MC, Bacci A (2020) Alterations of specific cortical GABAergic circuits underlie abnormal network activity in a mouse model of down syndrome. Elife 9:1–54.

Zurek AA, Yu J, Wang DS, Haffey SC, Bridgwater EM, Penna A, Lecker I, Lei G, Chang T, Salter EWR, Orser BA (2014) Sustained increase in α5GABAareceptor function impairs memory after anesthesia. J Clin Invest 124:5437–5441.

Figure Legends

Figure 1: GFP-positive neurons in X98 mice are SST-expressing MCs.

878 **A:** Top panels: Low magnification confocal micrograph of a triple immune-staining against SST
879 (magenta), PV (yellow) and GFP (cyan) in X98 coronal somatosensory slices. Bottom panels: detail of
880 L2/3 expression of the same markers shown in A. Inset in the right panel shows high magnification
881 examples of PV-positive, SST- only and both SST- and GFP-positive cells. **B:** Quantification of cells
882 expressing PV, SST or SST and GFP in L2/3. **C:** Morphological reconstructions of all GFP-positive
883 neurons filled with biocytin. **D**: Detail of an X98 MC axonal and dendritic interlayer distribution. Blue:
884 dendrites; red: axons. **E**: Axonal (red) and dendritic (blue) polar plots of the cell in D. **F:** Population
885 data of axon (red) and dendrite (blue) lengths distribution in L1 and L2/3 (n=10). Scale bars: 100 µm;
886 inset: 10 µm. ** $p<0.01$ and *** $p<0.001$.

887

888 **Figure 2: X98 GFP-positive neurons display distinct electrophysiological characteristics of**
889 **Martinotti cells.**

890 **A:** Representative current-clamp recordings from a GFP-expressing IN (green) and a PV cell (red) in
891 X98 mice. X98 GFP cells display a characteristic sag in response to hyperpolarizing current injection
892 and a highly adapting firing behavior. Conversely, PV-cells show fast-spiking patterns in response to
893 depolarizing current injections. **B:** Summary graphs of resting membrane potential (left), membrane
894 resistance (middle) and adaptation index (right) in PV INs (n=14) and MCs (n=22). **C:** Schematic of
895 mutually connected MC-PN and PV-PN pairs. **D:** Representative averaged voltage-clamp trace of
896 uEPSCs evoked by 5 APs at 50Hz in a PN, and recorded in a GFP-positive cell (green, upper panel) and
897 in a PV-cell (magenta, bottom panel) from a X98 mouse. **E:** Left panel: pooled normalized amplitudes
898 of uEPSC evoked with a 50Hz, 5 AP train. Right: population plot of PPR of X98 GFP (n=20, green) and
899 PV-INs (n=11, red). **F:** Left: overlapped representative uIPSCs elicited by MCs (green) and PV-INs (red)
900 and recorded from PNs. Right: population plot of the uIPSC mean rise time from MC to PN (green)
901 and PV to PN (red) synapses. * $p<0.05$, ** $p<0.01$, *** $p<0.001$.

902

Figure 3: X98 MCs make axo-somatic contacts onto L2/3 PV-, VIP- and L1-INs but not PNs.

A: Confocal micrographs of X98 L2/3 somatosensory cortex slices immunostained against PV (blue), GFP (green), and Gephyrin (magenta) or **B:** PV (blue), GFP (green), and vGAT (magenta). **C:** Number of X98 MC contacts onto L2/3 PV INs. Distribution of the number of GFP- and vGAT-positive puncta per PV-positive soma. **D:** Confocal micrographs of L2/3 somatosensory cortex slices immunostained against TdTomato (pseudocolored in blue), GFP (green), and gephyrin (magenta) or **E:** TdTomato (blue), GFP (green), and vGAT (magenta) in VIPcre::X98 mice infected with AAV.flex.tdTomato. **F:** Number of X98 MC contacts onto L2/3 VIP INs. Distribution of the number of GFP- and vGAT-positive puncta juxtaposed to the soma of VIP INs. **G:** L1 X98 somatosensory cortex slice immunostained against GFP (green), VGAT (magenta) and gephyrin (blue) or **H:** GFP (cyan), VGAT (magenta) and NeuN (yellow). **I:** Distribution of the number of GFP- and vGAT-positive puncta juxtaposed to the soma of L1 INs. The histogram shows the distribution of the number of GFP- and vGAT-positive puncta per L1 NeuN-positive soma. **J:** L2/3 X98 somatosensory cortex slice immunostained against GFP (green), vGAT (magenta) and PV (blue) or **K:** GFP (cyan), VGAT (magenta) and NeuN (yellow). **L:** Number of GFP- and vGAT-positive puncta juxtaposed to the soma of L2/3 NeuN-positive, putative PNs. Distribution of the number of GFP- and vGAT-positive puncta per soma of L2/3 NeuN-positive, putative PN. * in G and J panels indicates the immunolabelling gap produced by unlabeled somas. Scale bars: 5 µm.

Figure 4: Diversity of X98 MC connectivity onto different neuronal types in the L2/3 of somatosensory cortex.

A: Schematic representation of the tested inhibitory connections involving MCs. **B**: Representative voltage-clamp uIPSC average traces from MC to PN (black), PV(magenta), L1 (orange) and VIP (blue)INs. Gray dotted line represents the time of the peak of presynaptic action potentials. **C**: Representative distributions of uIPSC Rt recorded from individual MC-PN (black), MC-PV (magenta),

928 MC-L1 (orange), and MC-VIP (blue) connections. **D**: uIPSC (same as in C) normalized to the peak. **E**:
929 Population plot of the mean uIPSC amplitudes from individual MC-PN, MC-PV, MC-L1, and MC-VIP
930 recorded connections. **F**: Population plot of the mean uIPSC Rts from individual MC-PN, MC-PV, MC-
931 L1, and MC-VIP recorded connections. G: Pie charts illustrating the connectivity rates of MC-MC, MC-
932 L1, MC-VIP, MC-PV, and MC-PN synapses. ** p<0.01, *** p<0.001.

933

934 **Figure 5: Plasticity of x98 MC-mediated synaptic inhibition in L2/3 of somatosensory cortex.**

935 **A:** Schematic representation of the tested inhibitory circuits involving MCs. **B:** Representative
936 voltage-clamp averaged traces of uIPSCs from MCs onto PNs (black), PV (magenta), L1 (orange) and
937 VIP (blue) INs. **C:** Normalized uIPSC amplitudes elicited by MCs onto different elements of the L2/3
938 inhibitory circuit. Inhibition of MCs onto PN (black) and L1 INs (orange) is strongly depressing,
939 whereas MC connections onto VIP (blue) INs are facilitating. The strength of MC-PV synapses was
940 overall unchanged during repetitive presynaptic stimulations. *** p < 0.001.

941

942 **Figure 6: α5-GABA$_A$Rs mediate synaptic inhibition selectively from X98 MCs.**

943 **A:** Schematic representation of paired recordings between a MC or PV and a PN. **B:** Top left,
944 representative average uIPSC traces elicited by a PV onto a PN in the absence (black) and presence
945 (grey) of zolpidem. Traces are scaled to highlight zolpidem effect on uIPSC decay time. Bottom left,
946 population data of zolpidem effect on the weighted decay time constant ($\tau_{d,w}$, left). Top right:
947 representative average uIPSC traces elicited by a PV cell onto a PN in the absence (black) and
948 presence (blue) of α5IA. Bottom right, population data of α5IA effect on uIPSC amplitudes in PV-PN
949 pairs. **C:** Same as in B but for MC-PN pairs. **D:** Representative voltage-clamp traces of sIPSCs
950 recorded from a PN before (control, black) and after 15 minutes incubation with 100 nM α5IA (blue).
951 MC-PN synapse uIPSCs recorded with non-physiological, Cs-based, high chloride, internal solution
952 (see methods). **E:** Representative averaged traces of fast (top) and slow (bottom) events recorded

from the PN in D. Only amplitudes of slow events are affected by α5IA (blue trace, bottom panel). **F:** Population plot of individual cells, fast and slow sIPSC median amplitudes measured in control and after incubation with α5IA. *p<0.05, **p<0.01.

Figure 7: Inhibitory synaptic transmission involving MCs and other INs does not rely on α5-$GABA_A$Rs.

A: Schematic representation of the tested inhibitory circuits involving MCs. **B:** Representative averaged voltage-clamp traces of uIPSCs from MCs onto different element of the circuit and from VIP to MC before (black) and after (blue) application of α5IA. **C:** Population data of uIPSC amplitude before (Ctrl) and 15 minutes after α5IA application.

Figure 8: α5$GABA_A$Rs only contribute to tonic inhibition in L2/3 PN of mouse somatosensory cortex.

A: Whole-cell voltage-clamp recordings from L2/3 PNs preincubated with either vehicle (aCSF, left) or α5IA (right). DNQX (10 μM) and GABA (5 μM) were continuously present in both conditions. Orange areas (ΔI_{hold}) represent tonic inhibition measured after gabazine onset. Insets: All-points histograms of the current trace obtained in the absence (grey and blue histograms) and presence of gabazine (black histograms). Gaussian fits were used to determine the noise half-width. **C-E:** same as in A for MCs and PV-INs, correspondingly. **B-D-F:** Population graphs of holding-current shifts after gabazine application (ΔI_{hold}). * p<0.05.

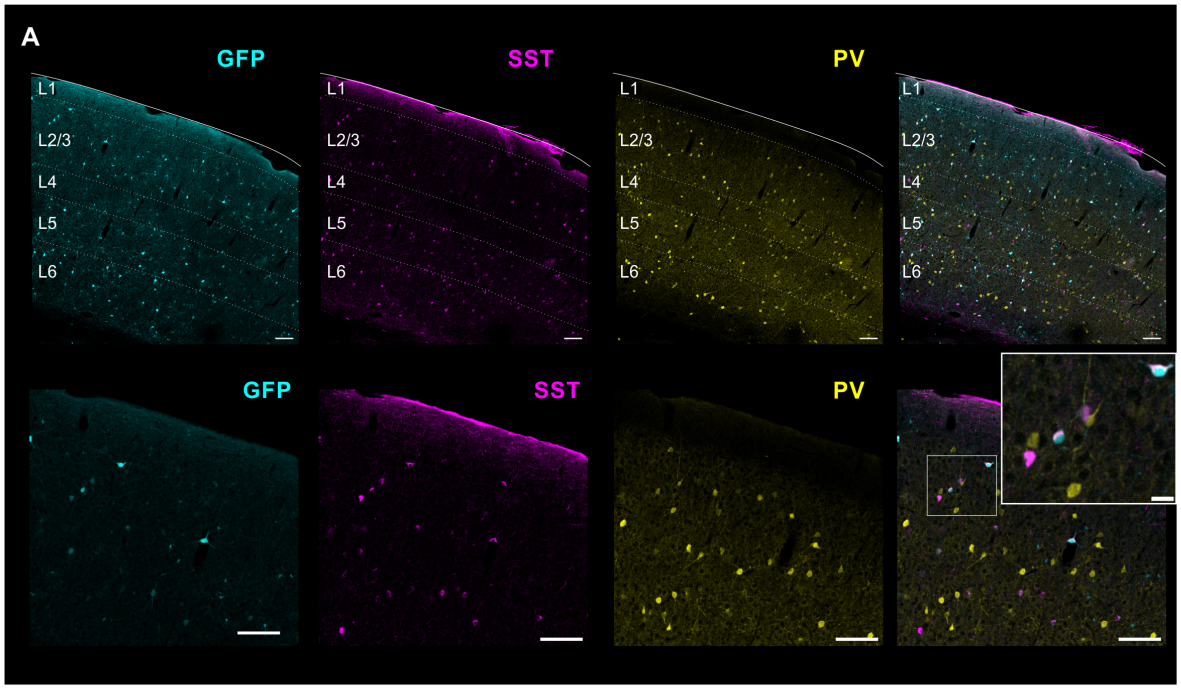

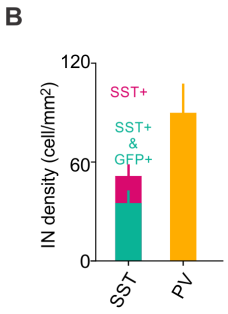

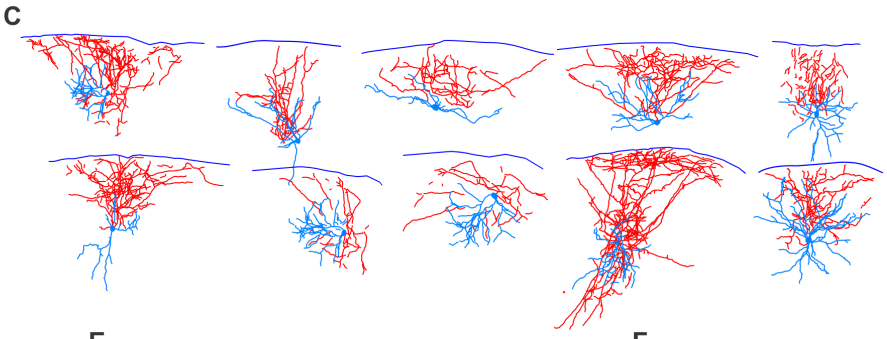

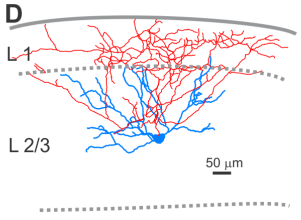

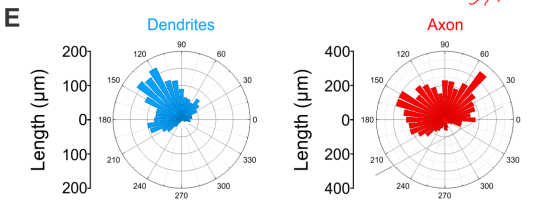

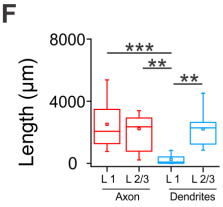

Donato et al. - Figure 1

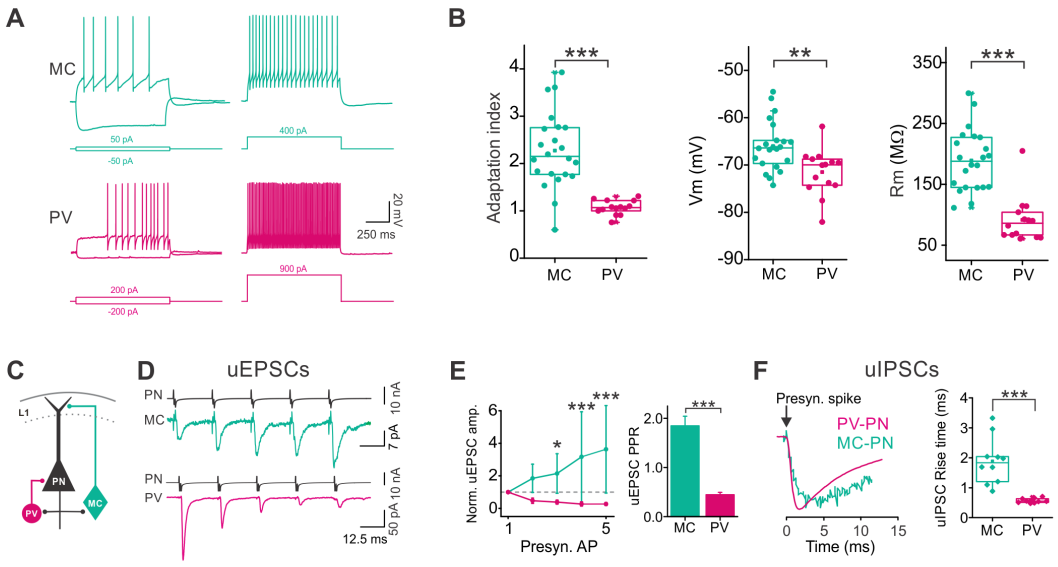

Donato et al. - Figure 2

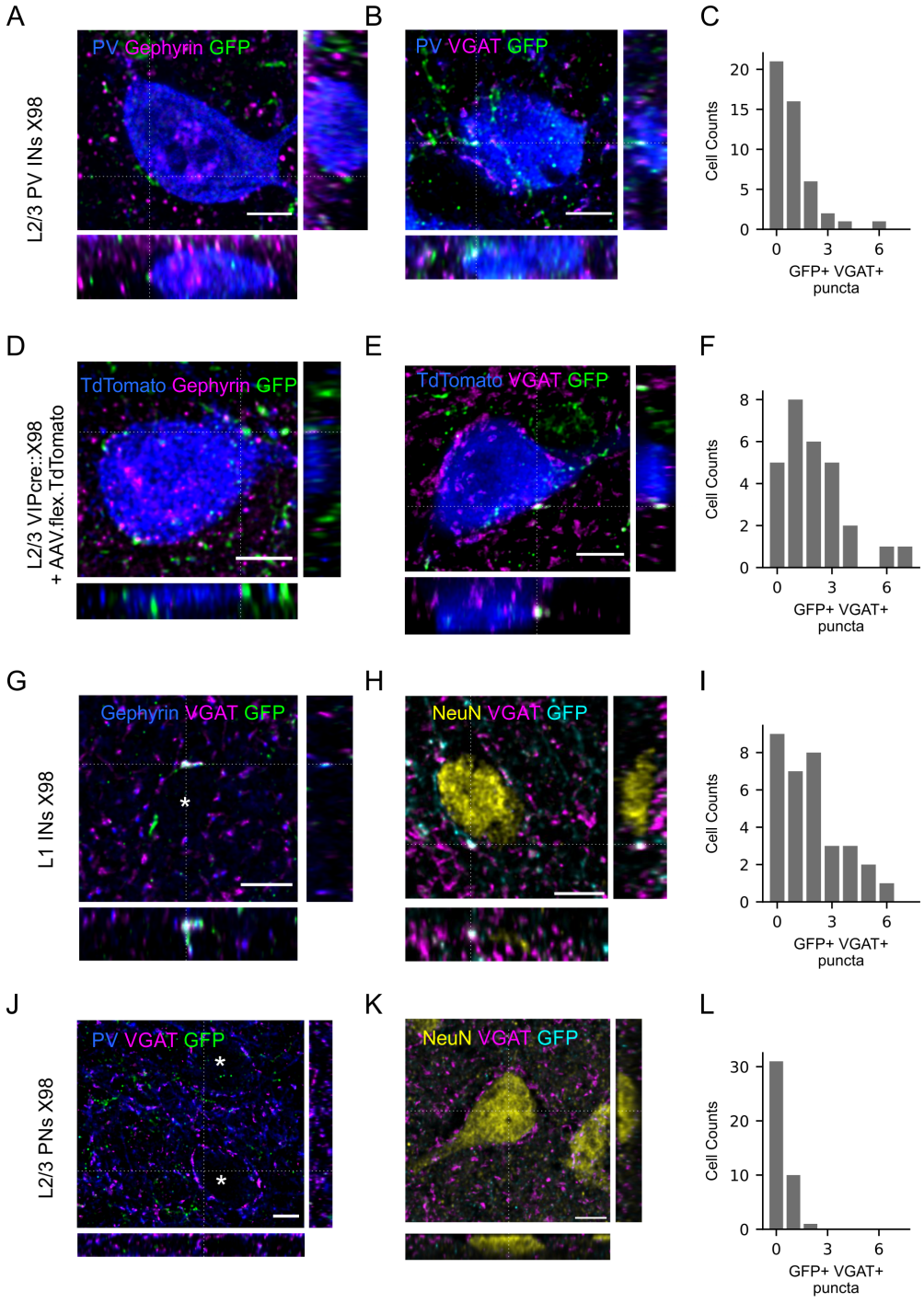

Donato et al. - Figure 3

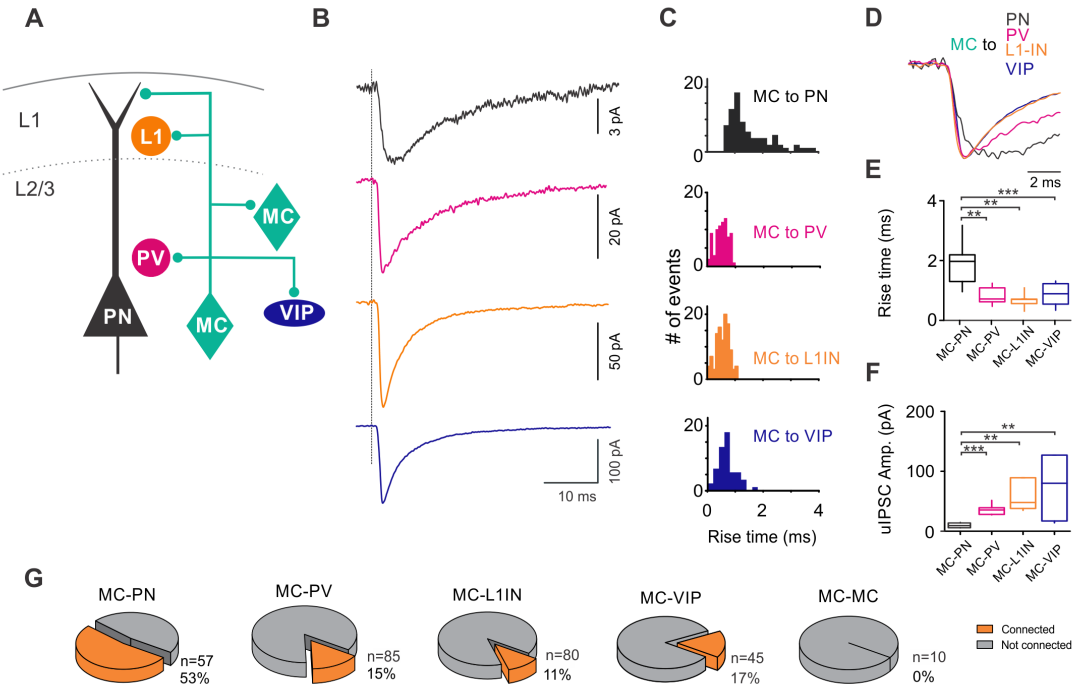

Donato et al. - Figure 4

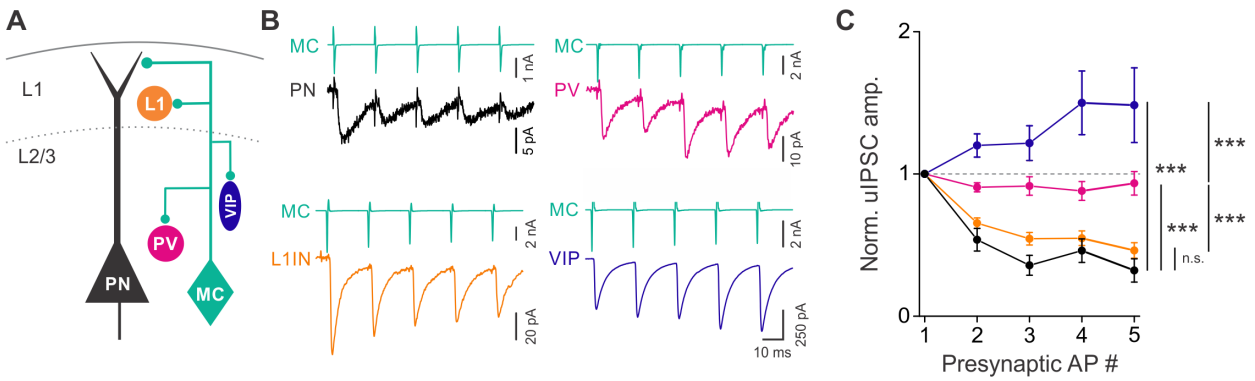

Donato et al. - Figure 5

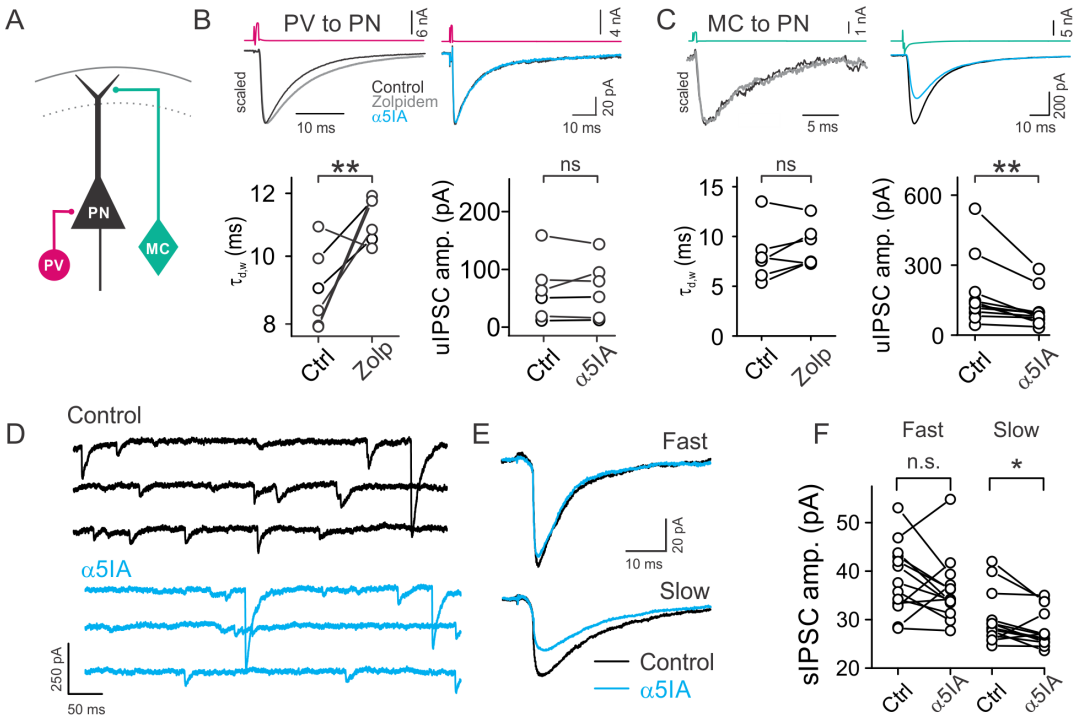

Donato et al. - Figure 6

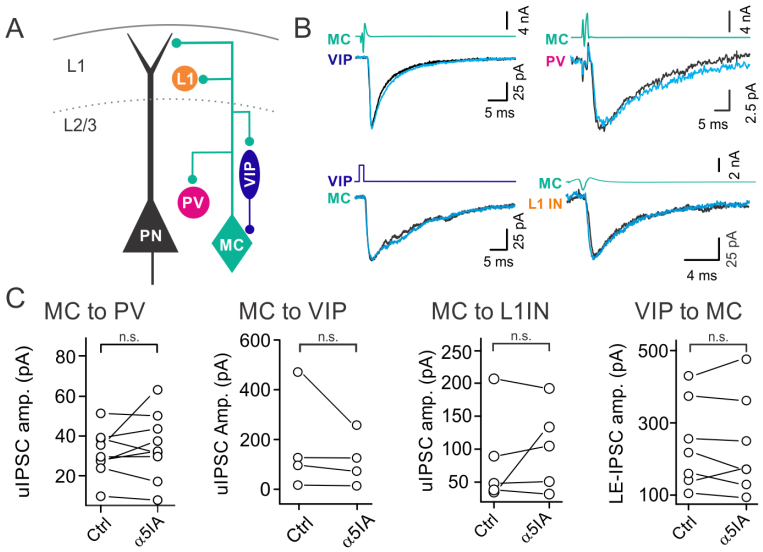

Donato et al. - Figure 7

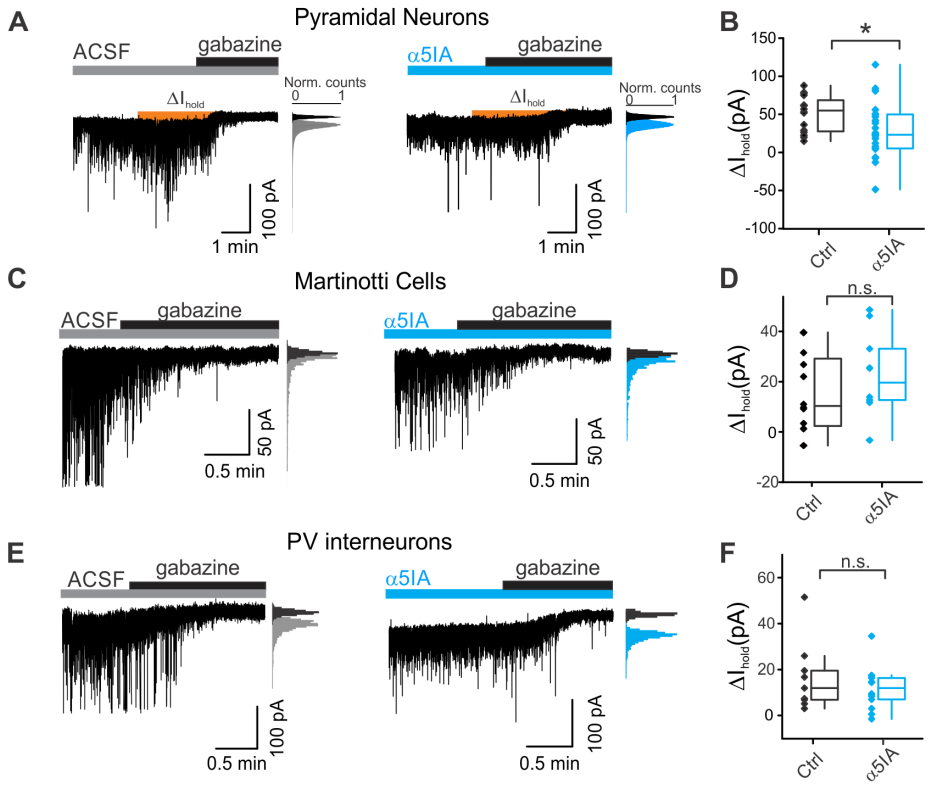

Donato et al. - Figure 8